NASA TECHNICAL MEMORANDUM

NASA TM X-915

AERODYNAMIC CHARACTERISTICS OF A MANNED LIFTING ENTRY VEHICLE AT A MACH NUMBER OF 6.8

by Charles L. Ladson

Langley Research Center
Langley Station, Hampton, Va.

NATIONAL AERONAUTICS AND SPACE ADMINISTRATION • WASHINGTON, D. C. • FEBRUARY 1964

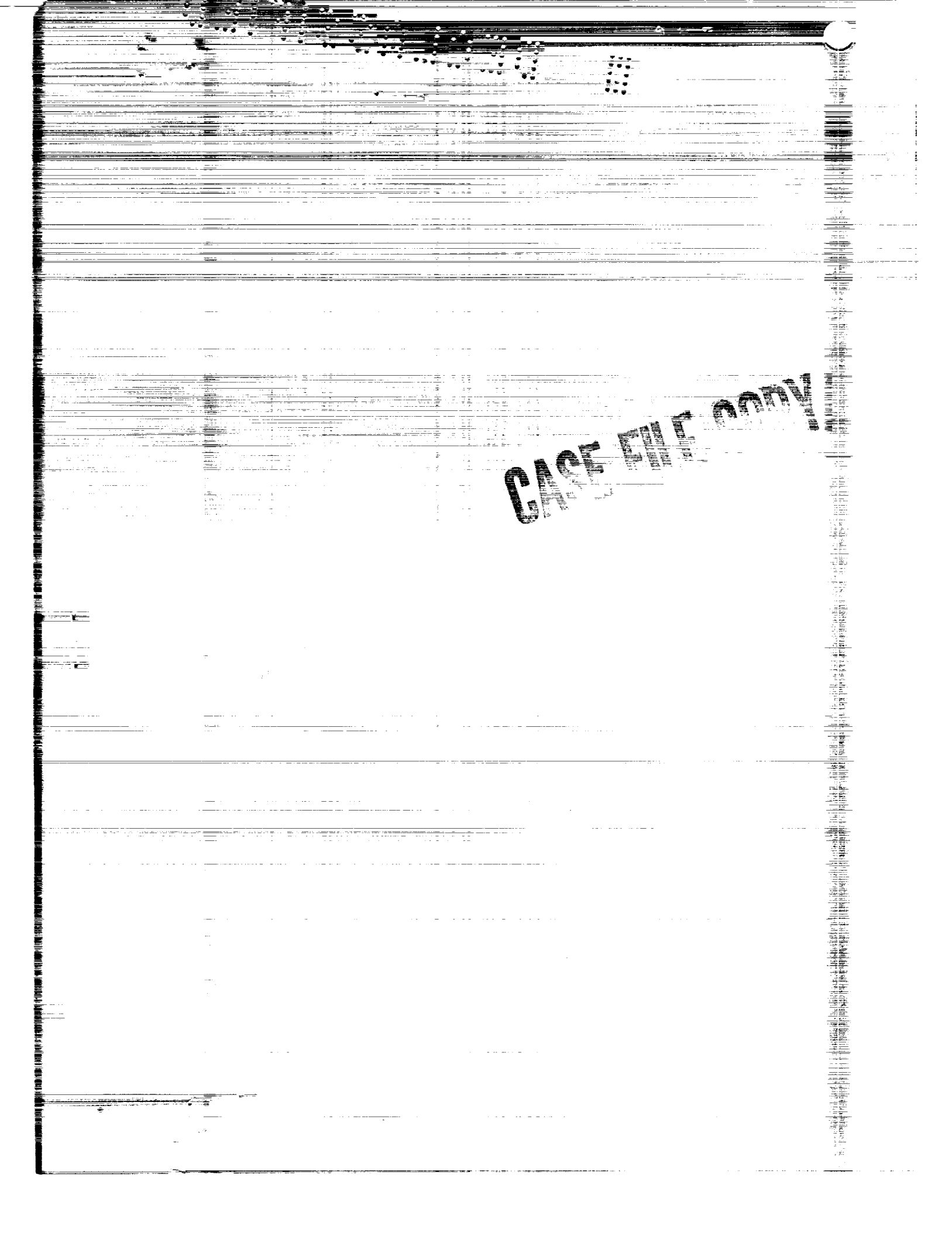
CASE EXIT only

AERODYNAMIC CHARACTERISTICS OF A MANNED LIFTING ENTRY VEHICLE AT A MACH NUMBER OF 6.8

By Charles L. Ladson

Langley Research Center
Langley Station, Hampton, Va.

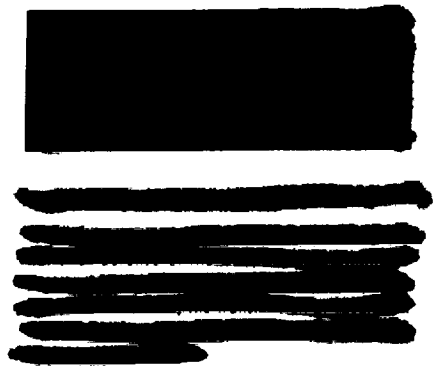

NATIONAL AERONAUTICS AND SPACE ADMINISTRATION

AERODYNAMIC CHARACTERISTICS OF A MANNED LIFTING ENTRY VEHICLE AT A MACH NUMBER OF 6.8*

By Charles L. Ladson

12612

SUMMARY

A

The aerodynamic characteristics of a cambered flat-bottom vehicle, designated HL-10 (horizontal lander 10), with a blunt-leading-edge delta planform and with a hypersonic lift-drag ratio of about 1 are being studied. Several fins in combination with the HL-10 configuration have been studied at a Mach number of 6.8 to determine the relative fin contribution to the aerodynamic characteristics (notably, directional stability). The results indicate that tip dorsal fins rolled out 60° from the horizontal had the most desirable aerodynamic characteristics. With these fins the model was directionally and laterally stable throughout the trim range of lift coefficient from 0.20 to 0.48. The trimmed lift-drag ratios at these lift coefficients are 1.25 and 0.78, respectively.

conf.

AUTHOR

INTRODUCTION

An investigation has been undertaken at the Langley Research Center to determine the aerodynamic characteristics and problems of a manned lifting entry vehicle having a maximum hypersonic lift-drag ratio of about 1. After an extensive review of configuration types, two vehicle shapes were selected for study. The configuration concepts and some preliminary aerodynamic data on these configurations at a Mach number of 6.8 are presented in reference 1. Low-subsonic-speed data on these configurations have also been published in reference 2. From these results at subsonic and hypersonic speeds, one configuration, designated HL-10 (horizontal lander 10) has been selected for further tests throughout the Mach number range.

The HL-10 configuration as reported in reference 1 had vertical tip tails for directional stability which was achieved at a Mach number of 6.8. At subsonic speeds, however, reference 2 shows that these tip fins created a local flow separation and thus were not only ineffective in providing the vehicle with directional stability but also caused a negative incremental pitching moment. It was also shown in reference 2 that a center vertical fin was one means of providing subsonic directional stability. In addition, the subsonic drag and incremental pitching moments were reduced, and a significantly higher

---

*Title, Unclassified.

trimmed maximum lift-drag ratio was achieved. Inasmuch as this center fin alone would not suffice at high angles of attack at hypersonic speeds, an investigation was undertaken in the Langley 11-inch hypersonic tunnel to design a fin arrangement suitable for both subsonic and hypersonic speeds.

Several model modifications were studied during the tests, including lower surface dihedral, tip ventral fins, single center-line dorsal and ventral fins, and tip-fin roll-out. The tests were conducted at a Mach number of 6.8 at angles of attack up to about 70° and at free-stream Reynolds numbers of 0.17×10^6 and 0.23×10^6 per inch. Longitudinal and directional stability and control data are presented with limited analysis.

SYMBOLS

b	span
C_A	axial-force coefficient, Axial force/qS
C_D	drag coefficient, Drag/qS
C_L	lift coefficient, Lift/qS
C_l	rolling-moment coefficient, Rolling moment/qSb
C_{l_β}	rate of change of rolling-moment coefficient with angle of sideslip at zero sideslip angle, $\left(\partial C_l/\partial\beta\right)_{\beta=0}$, per deg
C_m	pitching-moment coefficient about moment center at $0.53l$, Pitching moment/qSl
C_N	normal-force coefficient, Normal force/qS
C_n	yawing-moment coefficient about moment center at $0.53l$, Yawing moment/qSb
C_{n_β}	rate of change of yawing-moment coefficient with angle of sideslip at zero sideslip angle, $\left(\partial C_n/\partial\beta\right)_{\beta=0}$, per deg
C_Y	side-force coefficient, Side force/qS
C_{Y_β}	rate of change of side-force coefficient with angle of sideslip at zero sideslip angle, $\left(\partial C_Y/\partial\beta\right)_{\beta=0}$, per deg
L/D	lift-drag ratio
l	model length

[redacted]

M	free-stream Mach number
q	free-stream dynamic pressure
S	planform area, including area of elevons
S_e	elevon planform area
X,Y,Z	body axes
α	angle of attack, deg
β	angle of sideslip, deg
δ_e	elevon deflection angle, positive with trailing edge down, deg; used with subscripts L and R to indicate left elevon deflection and right elevon deflection, respectively
ϕ	fin roll-out angle, normal to leading edge, deg

MODELS AND DESIGNATIONS

Three-view drawings showing details of the HL-10 configuration are presented in figure 1(a). The body cross-section ordinates are presented in reference 1. Sketches of the various fin and body shapes tested in place of the original tip dorsal fins are shown in figure 1(b). The fins and bodies are identified as follows:

Fin A: Tip dorsal fins toed-in 16° (fig. 1(a))

Fin B: Tip ventral fins toed-in 16° (fig. 1(b))

Fin C: Center-line ventral fin extending aft of body base (fig. 1(b))

Fin D: Tip dorsal fins toed-in 16° and rolled out 60° from the horizontal

Fin E: Center-line dorsal fin used in reference 2 (fig. 1(b))

Basic body: Original body with no fins, as in reference 1 (fig. 1(a))

Dihedral body: Basic body with dihedral added to lower surfaces aft of $0.59l$ (fig. 1(b))

Photographs of several of the configurations tested are presented in figure 2.

All dimensions presented in figure 1 are for a model having a length of 8 inches. This model was constructed of stainless steel and was equipped with interchangeable fins and elevons. As mentioned in reference 1, this model caused a tunnel blockage problem at angles of attack above about 40°. In order that the data presented at the higher angles of attack be obtained a model was

[redacted]

constructed with a length of 4.5 inches. As seen in the schlieren flow photographs (fig. 3), this size model did not create a tunnel blockage problem. (See fig. 3(e).)

All coefficients are based on the total projected planform area, the span, and the length of the model. The moment center is located 0.53l behind the vehicle nose and 0.0125l below the reference center line. The reference areas and lengths are as follows:

S, sq in.	b, in.	l, in.
22.84 7.23	5.155 2.899	8.000 4.500

APPARATUS, TESTS, AND PROCEDURES

The data contained herein were obtained in the Mach 6.8 test section of the Langley 11-inch hypersonic tunnel. A description and calibration of this facility is presented in reference 3. At angles of attack from 0° to 30° and from 40° to 70°, the tests were conducted at an average stagnation pressure of about 20 atmospheres absolute at an average Mach number of about 6.87. At angles of attack between 30° and 40°, the stagnation pressure was about 15 atmospheres, and the average Mach number was about 6.82. All tests were conducted at a stagnation temperature of about 600° F. The Reynolds numbers at stagnation pressures of 15 and 20 atmospheres were 0.17×10^6 and 0.23×10^6 per inch, respectively.

The angles of attack of the model were measured optically by use of a light beam reflected onto a calibrated scale from a prism imbedded within the model surface. This method gave the true angle of attack of the model, including the deflection of the model and sting under load. The model base pressure was measured at angles of attack up to 40°. The base pressure contribution to axial force was compared with the measured axial force and found to be negligible. Thus, the data presented are uncorrected.

The forces and moments were measured on electrical strain-gage balances. Six-component data were obtained at angles of attack up to 40° for the 8-inch-long model. Above this angle of attack, the 4.5-inch-long model was used with a five-component balance (no axial force). In order that lift and drag coefficients above $\alpha = 40°$ be obtained, the axial force was plotted up to 40° and extrapolated to higher angles of attack with the aid of Newtonian theory. The contribution of C_A to C_m at these higher angles of attack was negligible. (Only the configurations with fins off and with fin D were tested above an angle of attack of 40°.)

All lateral and directional stability data were obtained at four angles of sideslip between 0° and 8°. Only the slopes have been presented. All

longitudinal performance data are referred to the stability-axis system, whereas the directional, lateral, and longitudinal stability results are referred to the body-axis system.

ACCURACY OF RESULTS

The accuracy in angles of attack and sideslip was ±0.1°. A summary of the average values and accuracies in Mach number and dynamic pressure and of the balance accuracy in terms of the aerodynamic coefficients is presented in the following table:

α, deg	M	q, lb/sq ft abs	Accuracy of static balance calibration in terms of -					
			C_N	C_A	C_m	C_l	C_n	C_Y
0 to 30	6.87 ± 0.03	376 ± 1.3	0.0026	0.0012	0.0003	0.0001	0.0002	0.0008
30 to 40	6.82 ± 0.03	294 ± 1.3	.0034	.0016	.0004	.0001	.0002	.0011
40 to 70	6.87 ± 0.03	376 ± 1.3	.0132		.0029	.0010	.0009	.0026

Mach number varied about ±0.03 and dynamic pressure varied about 6 lb/sq ft during each test as a result of a change in tunnel throat size due to heating as each test progressed. These variations were accounted for in the data reduction.

RESULTS

The basic longitudinal stability and control data for the various configurations are presented in figures 4 to 9, and the trim characteristics of configuration HL-10 with fin D are presented in figure 10. Directional and lateral stability and lateral control data are shown in figures 11 to 13.

The angle-of-attack range of the data for the configuration with tails off has been extended beyond that presented in reference 1, and the results are given in figure 4. The maximum trim angle of attack is seen to be about 56° with an elevon deflection angle of -60°. At hypersonic speeds, elevon effectiveness is essentially zero once an elevon is deflected beyond the streamwise direction so that it is shielded from the flow. Thus, this same trim angle of attack might be obtained with an elevon deflection angle of about -41°. Figure 11 shows that little change in directional and lateral stability for the configuration with tails off occurs at angles of attack above 40°. The characteristics of configuration HL-10 with fin A shown in figures 5 and 11 are from reference 1 and are presented here only for comparison.

The tip dorsal fins (fin A) used on configuration HL-10 caused a flow-separation problem about the upper surface at subsonic speeds (ref. 2), and this separation resulted in the configuration being directionally unstable. Reduced tip-fin toe-in angle helped to reduce the separation, but the configuration was not stable throughout the angle-of-attack range. Elimination of the tip fins and addition of a center-line dorsal fin resulted in adequate subsonic directional stability. This center-line fin is not sufficient for providing directional stability at hypersonic speeds because it is shielded from the flow at angles of attack above about 20°. Several fin configurations were investigated in order to provide hypersonic directional stability and still maintain directional stability at subsonic speeds. With fin B, the configuration was directionally stable (fig. 11) and, except for lower trim angles of attack due to the positive incremental lift of the fins (see figs. 6 and 7), the configuration had longitudinal characteristics similar to the HL-10 configuration with fin A. Examination of surface flow directions by use of oil-flow techniques indicated that a disturbance from the fin leading edge intersected the lower surface elevons. This shock could cause serious control and heating problems.

The lower surface of the configuration was modified to provide some dihedral in an effort to give additional directional stability. As seen in figure 11, the increment in directional stability obtained for the configuration with dihedral was small at the lower angles of attack. This configuration had the highest lift and lift-drag ratio of all configurations tested due to the increased lower surface slope; but since the additional lift is generated behind the center of gravity, it also has the lowest trim angle of attack (see fig. 7).

The use of a center-line ventral fin located aft of the wing trailing edge (fin C) was also investigated. This type of fin has the possibility of being stowed inside the vehicle base and, by being hinged downward, deployed when needed. Since the fin is located aft of the model base, it could cause no disturbances on the control surfaces. The fin could also be jettisoned easily, if necessary, at the lower speeds without possible damage to the vehicle. The stability and trim characteristics of the configuration with fin C are similar to those of the HL-10 with the dihedral body, but the lift coefficient is not as high (fig. 7). Figure 11 shows that with fin C, the HL-10 configuration was directionally unstable below an angle of attack of about 28°. A larger fin would be necessary to provide stability at these lower angles of attack but would also be difficult to store in the vehicle base prior to use.

The final and most promising fin modification tested was the tip dorsal fins rolled out 30° from the vertical along the wing leading edge. These tip fins (fin D) were tested both with and without the center-line dorsal fin (fin E). With fin D the HL-10 configuration has about the same level of directional stability as the original HL-10 configuration with fin A. (See fig. 11.) Adding the center-line dorsal fin has little effect on directional stability at $\alpha = 32°$ (fig. 12), as would be expected inasmuch as the fin is shielded, but it would probably show some gain at lower angles of attack. This center fin also had little effect on longitudinal characteristics, as seen by a comparison of results in figure 8.

The effects of elevon deflection on the longitudinal characteristics of the HL-10 with fin D are presented in figure 9(a) and are summarized in figure 10 for trim conditions. As seen in figure 10, in the angle-of-attack range between 20° and 52° the model has a trimmed lift capability from 0.20 to 0.48 and a trimmed L/D range from 1.25 to 0.78.

Lateral control characteristics are presented in figure 13 and the results are similar to those presented in reference 1. At low angles of attack the control effectiveness is small because of flow separation on the lower surface, but the effectiveness increases with increasing angle of attack. Since the lowest trimmed angle of attack is about 20°, low control effectiveness in the low angle-of-attack range is probably not important.

CONCLUDING REMARKS

The aerodynamic characteristics of a cambered flat-bottom vehicle, designated HL-10 (horizontal lander 10), with a blunt-leading-edge delta planform and with a hypersonic lift-drag ratio of about 1 are being studied. Several fins in combination with the HL-10 configuration have been studied at a Mach number of 6.8 to determine the relative fin contribution to the aerodynamic characteristics (notably, directional stability). The results indicated that tip dorsal fins rolled out 60° from the horizontal had the most desirable aerodynamic characteristics. With these fins the vehicle was directionally and laterally stable throughout the trim range of lift coefficient from 0.20 to 0.48, and the trimmed lift-drag ratios at these lift coefficients were 1.25 and 0.78, respectively.

Langley Research Center,
National Aeronautics and Space Administration,
Langley Station, Hampton, Va., December 10, 1963.

REFERENCES

1. Rainey, Robert W., and Ladson, Charles L.: Preliminary Aerodynamic Characteristics of a Manned Lifting Entry Vehicle at a Mach Number of 6.8. NASA TM X-844, 1963.

2. Ware, George M.: Aerodynamic Characteristics of Models of Two Thick 74° Delta Manned Lifting Entry Vehicles at Low-Subsonic Speeds. NASA TM X-914, 1964.

3. Bertram, Mitchel H.: Exploratory Investigation of Boundary-Layer Transition on a Hollow Cylinder at a Mach Number of 6.9. NACA Rep. 1313, 1957. (Supersedes NACA TN 3546.)

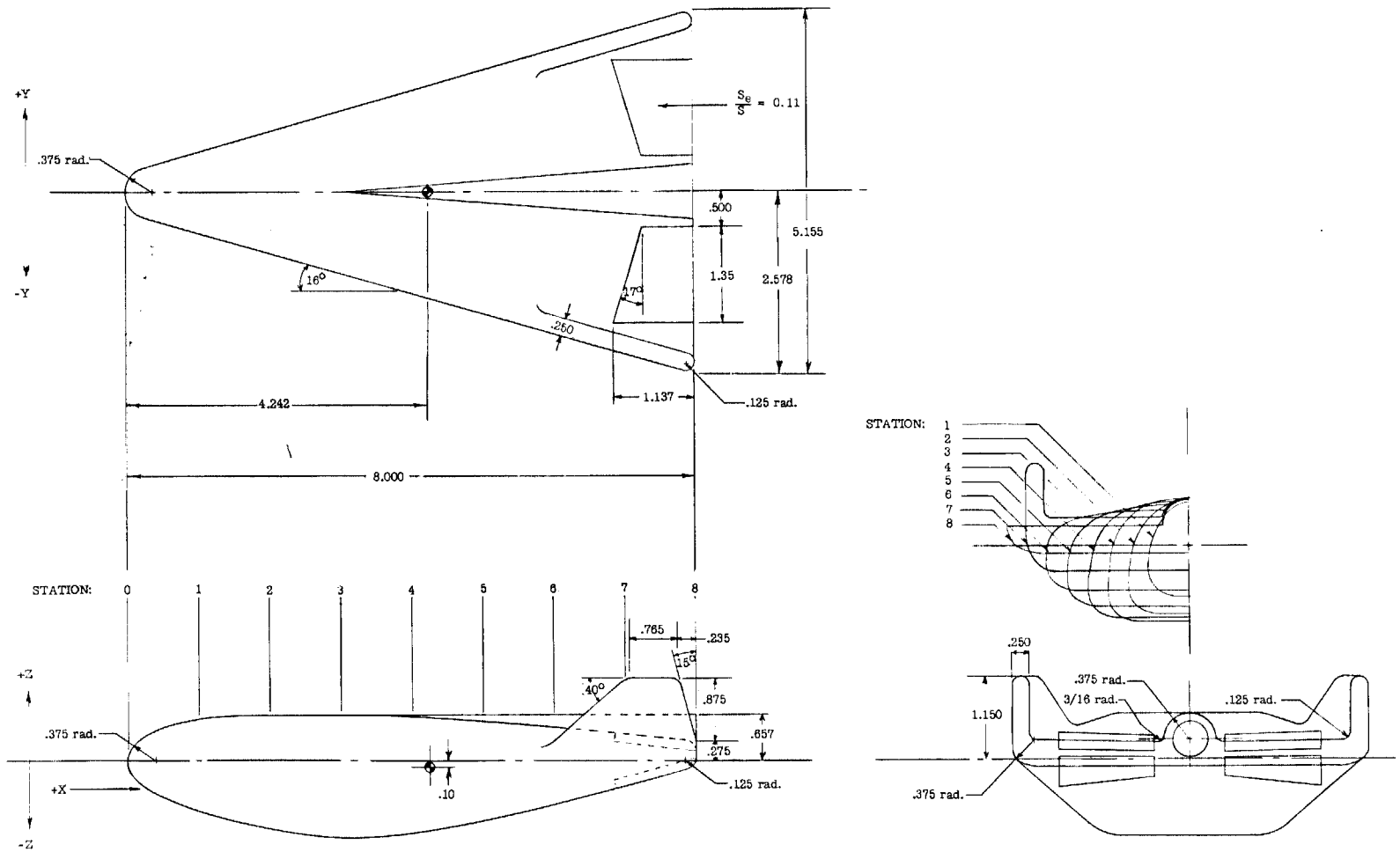

(a) Basic body with fin A.

Figure 1.- Model drawings and dimensions of HL-10. All linear dimensions are in inches.

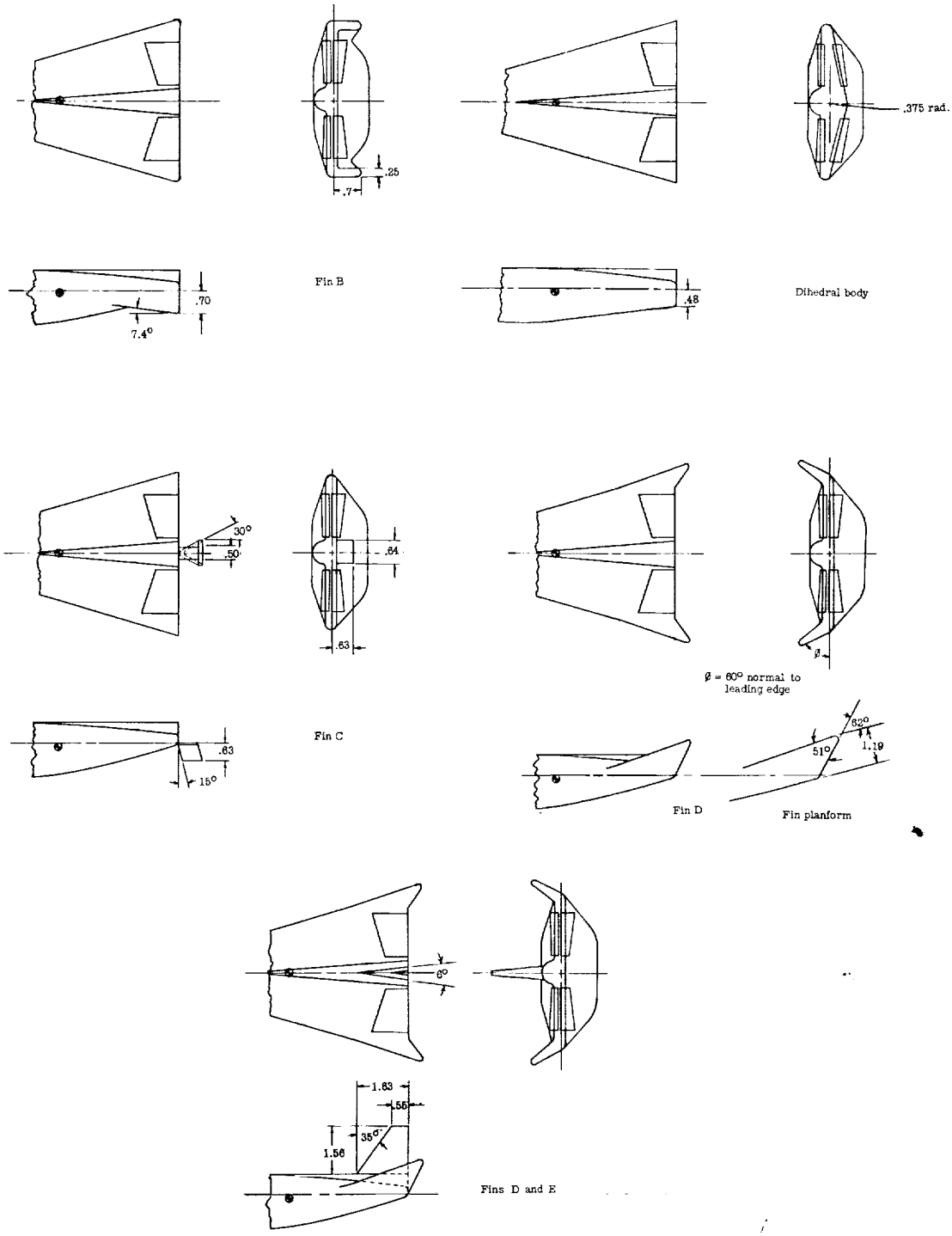

(b) Details of various fins and dihedral body.

Figure 1.- Concluded.

(a) Fin A.

L-63-5298

Figure 2.- Photographs of models with various fin configurations.

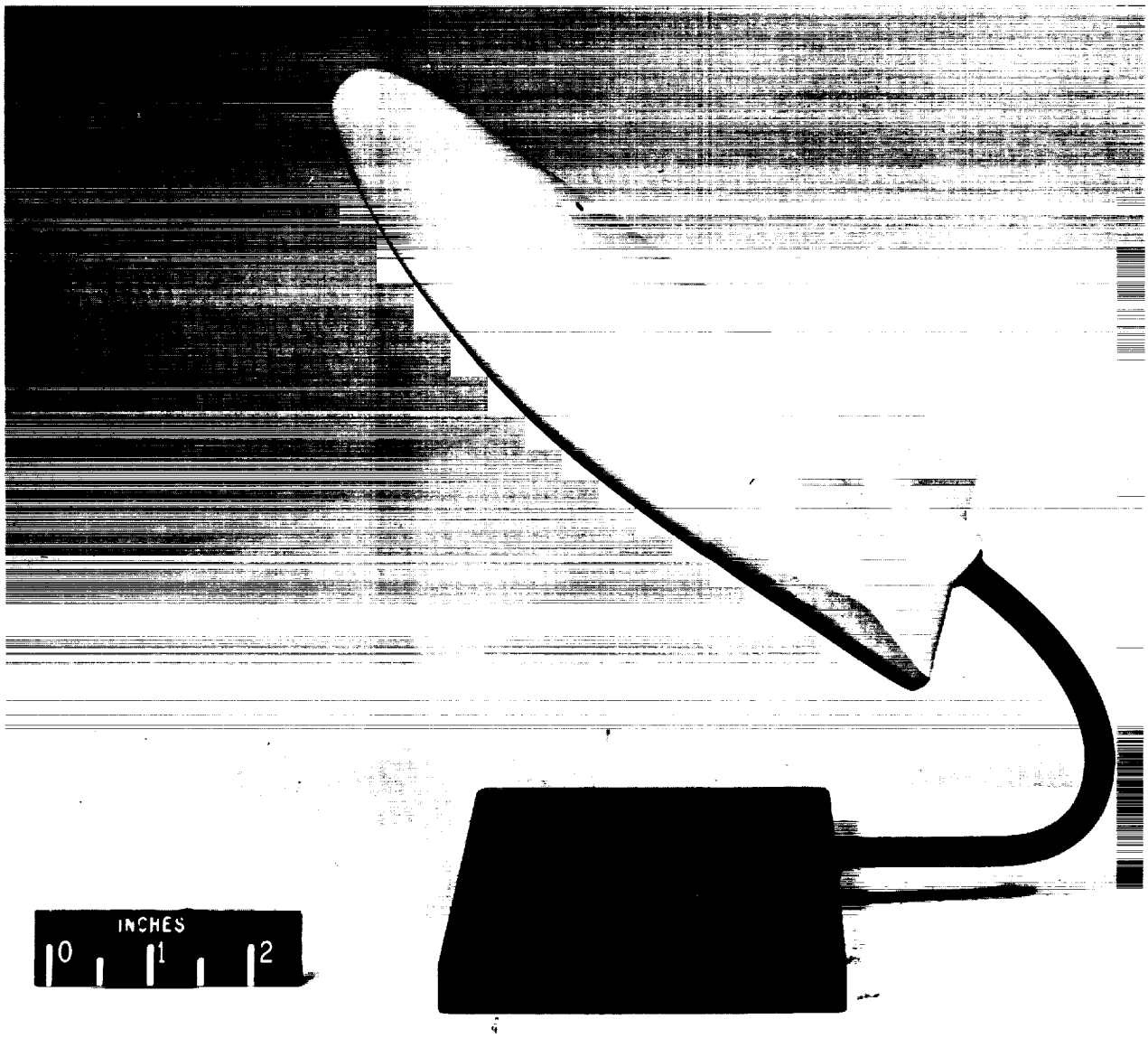

(b) Fins off. L-63-2082

Figure 2.- Continued.

(c) Fin B. L-63-5474

Figure 2.- Continued.

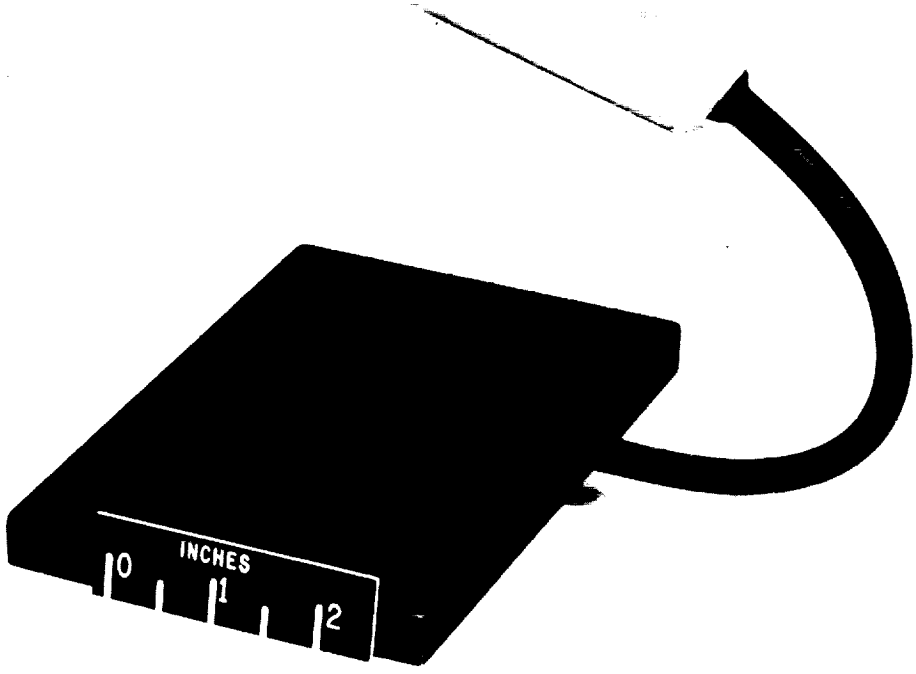

(d) Fin C. L-63-3639

Figure 2.- Continued.

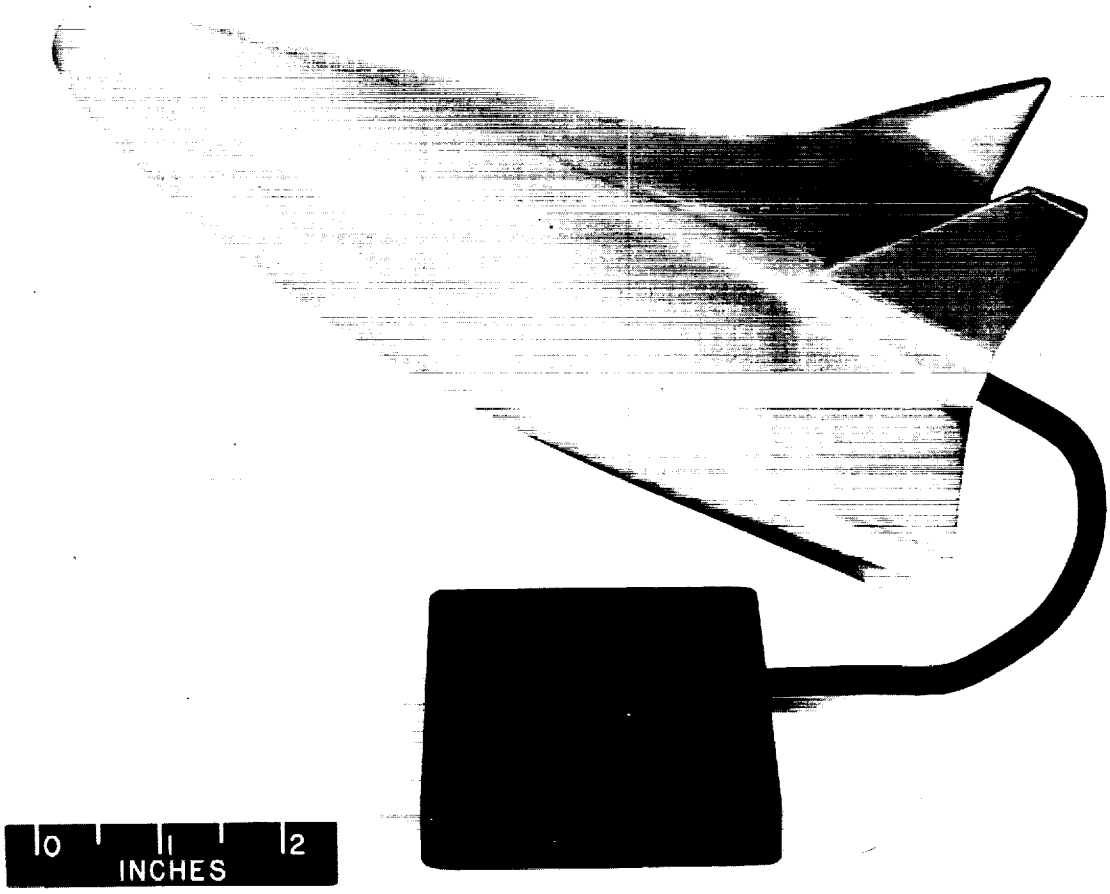

(e) Fins D and E. L-63-8151

Figure 2.- Concluded.

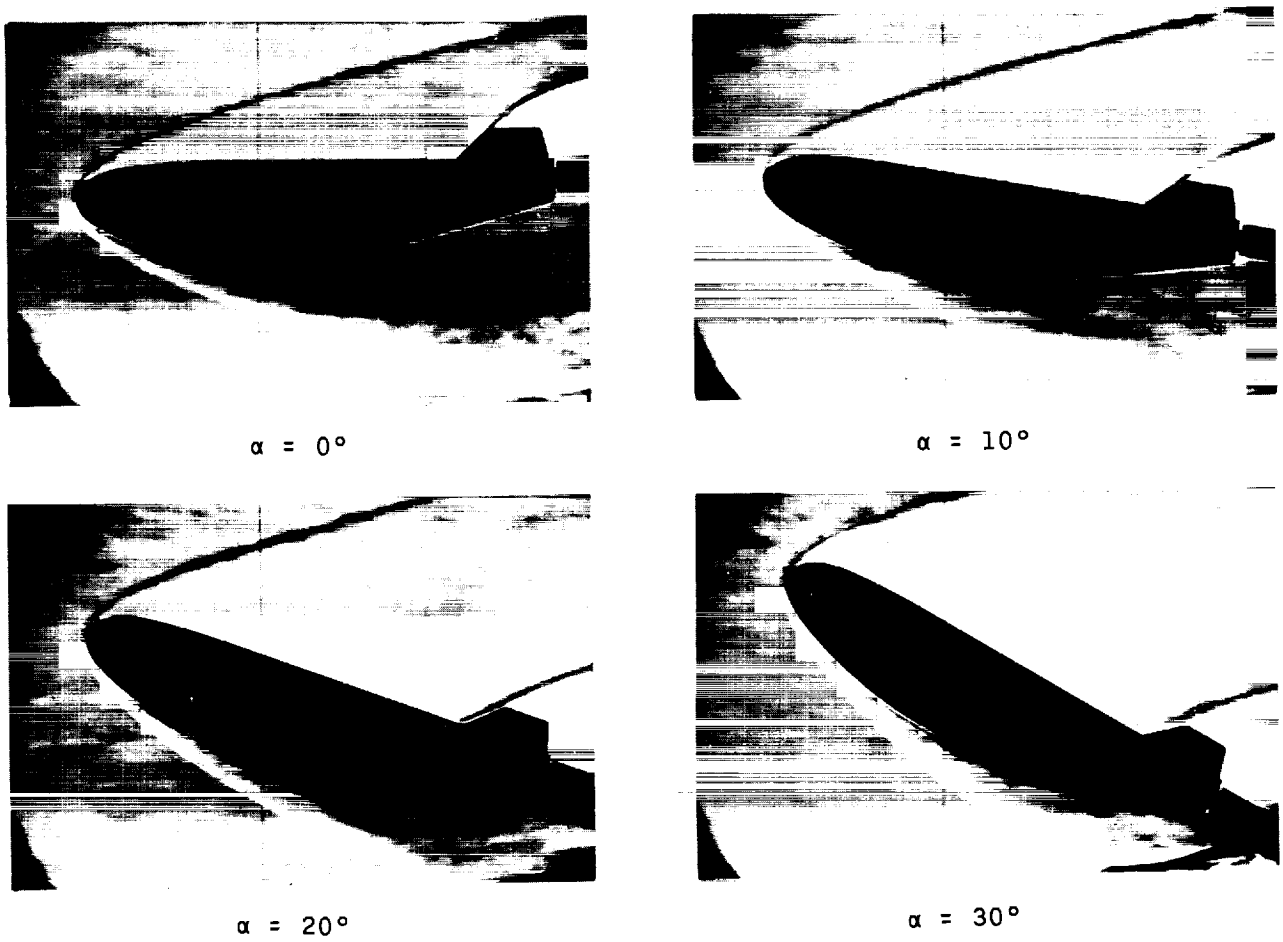

(a) Basic body with fin A. $\delta_e = 0^o$.

L-63-9252

Figure 3.- Schlieren flow photographs of various configurations.

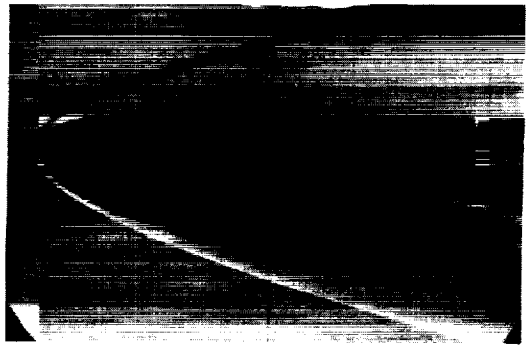

$\alpha = 0°$, $\delta_e = 30°$

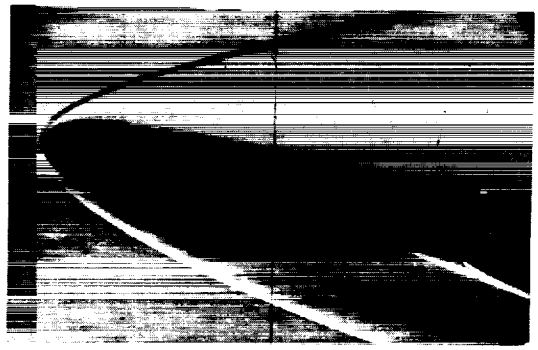

$\alpha = 10°$, $\delta_e = 30°$

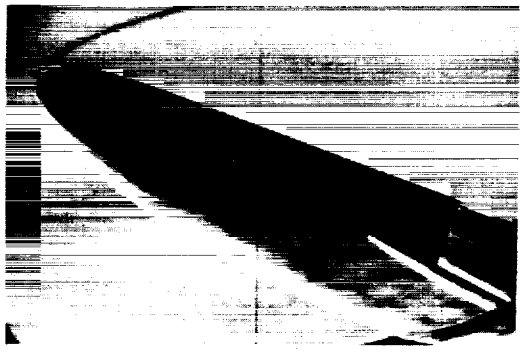

$\alpha = 20°$, $\delta_e = 15°$

$\alpha = 25°$, $\delta_e = 0°$

$\alpha = 35°$, $\delta_e = 0°$

(b) Basic body with fin B.

L-63-9253

Figure 3.- Continued.

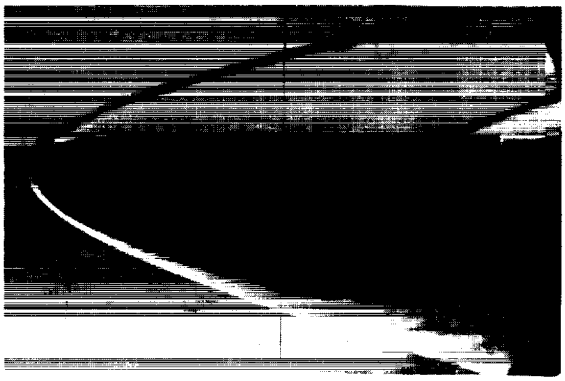

α = 0°

α = 25°

α = 30°

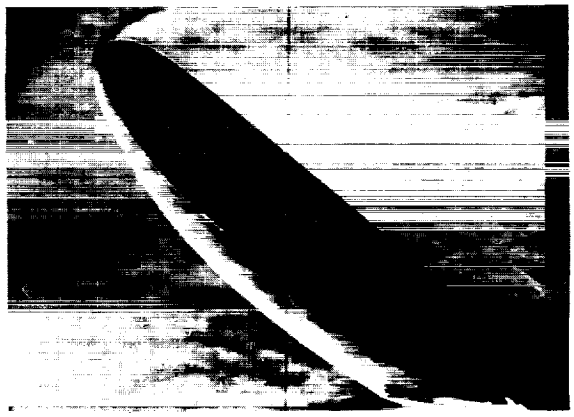

α = 40°

(c) Dihedral body with no fins. $\delta_e = 0^\circ$. L-63-9254

Figure 3.- Continued.

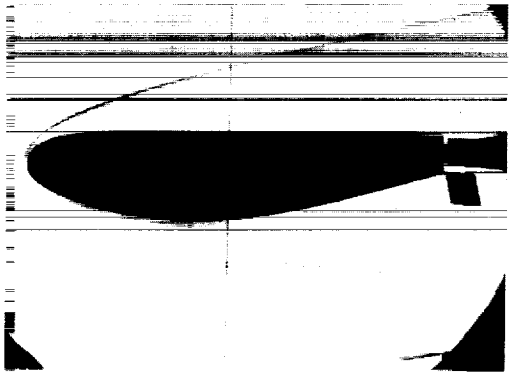

α = 0°

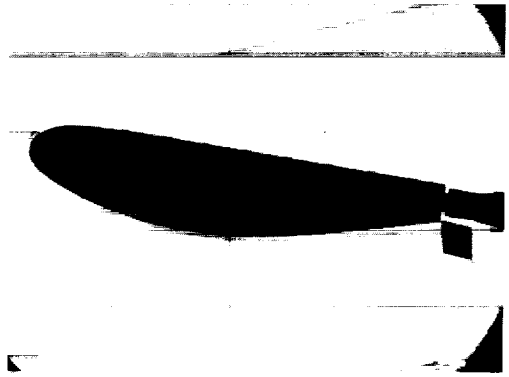

α = 10°

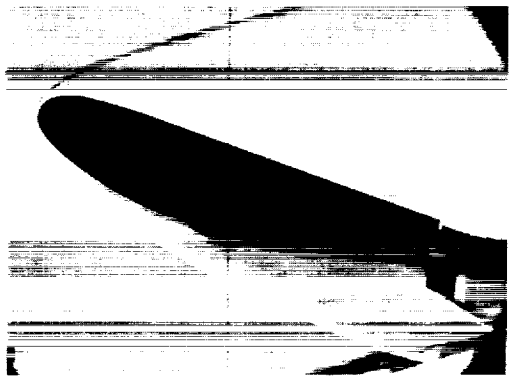

α = 20°

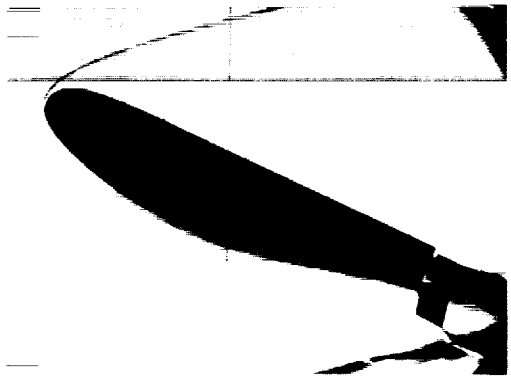

α = 25°

α = 30°

(d) Basic body with fin C. $\delta_e = 0°$. L-63-9255

Figure 3.- Continued.

$\alpha = 20°$, $\delta_e = 30°$

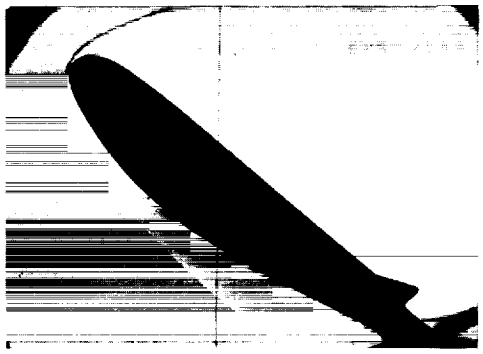

$\alpha = 40°$, $\delta_e = 0°$

$\alpha = 40°$, $\delta_e = 0°$

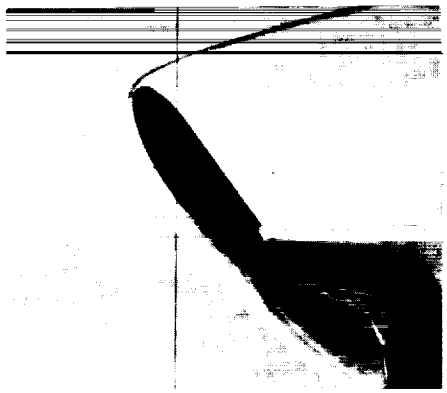

$\alpha = 55°$, $\delta_e = -60°$

$\alpha = 70°$, $\delta_e = -60°$

(e) Basic body with fin D. L-63-9256

Figure 3.- Continued.

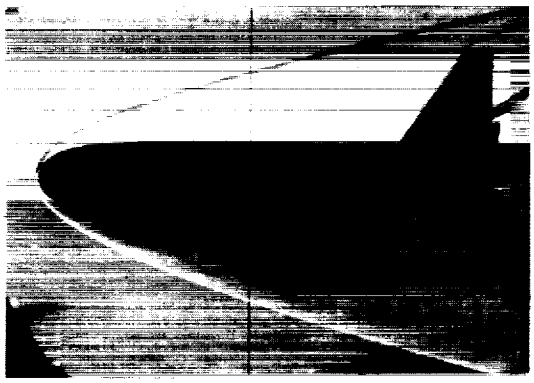

α = 0°

α = 10°

α = 20°

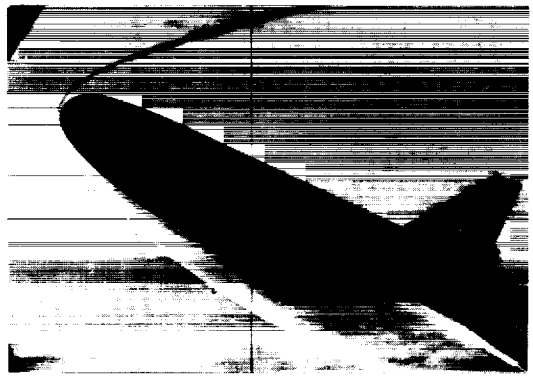

α = 25°

α = 35°

(f) Basic body with fins D and E. $\delta_e = 15°$. L-63-9257

Figure 3.- Concluded.

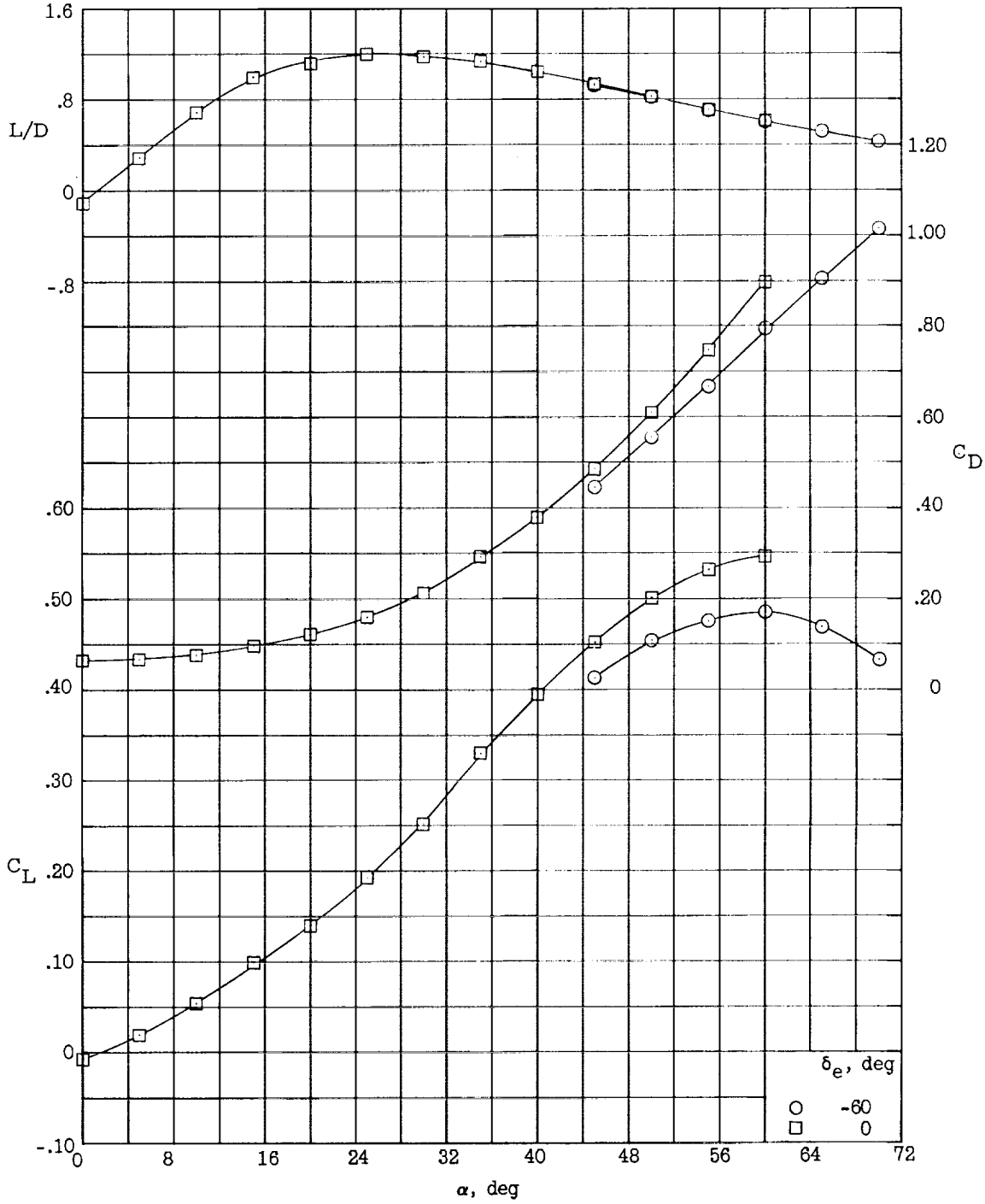

(a) Longitudinal performance characteristics.

Figure 4.- Longitudinal aerodynamic characteristics of configuration HL-10 with fins off.

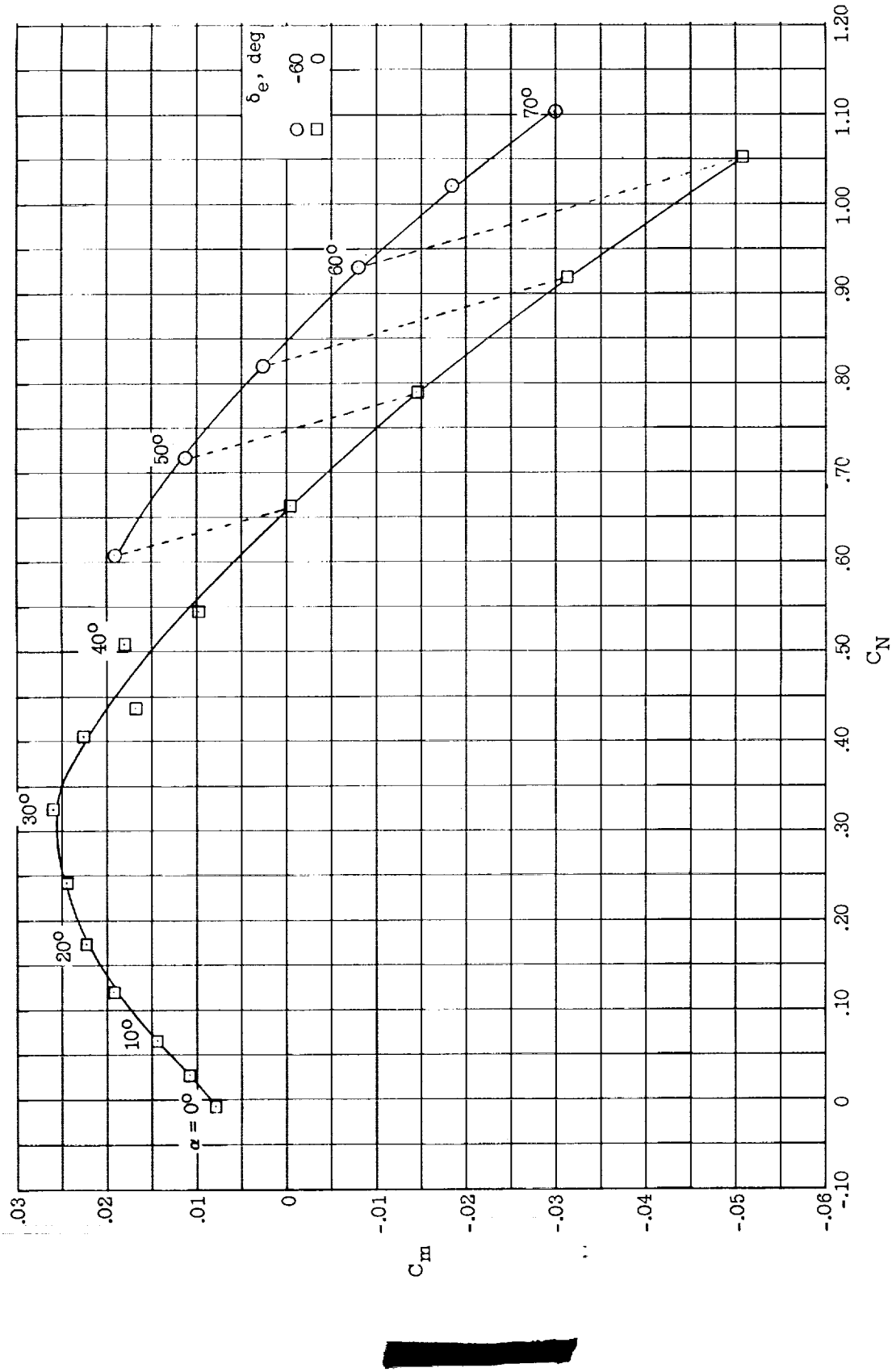

(b) Stability characteristics.

Figure 4.- Concluded.

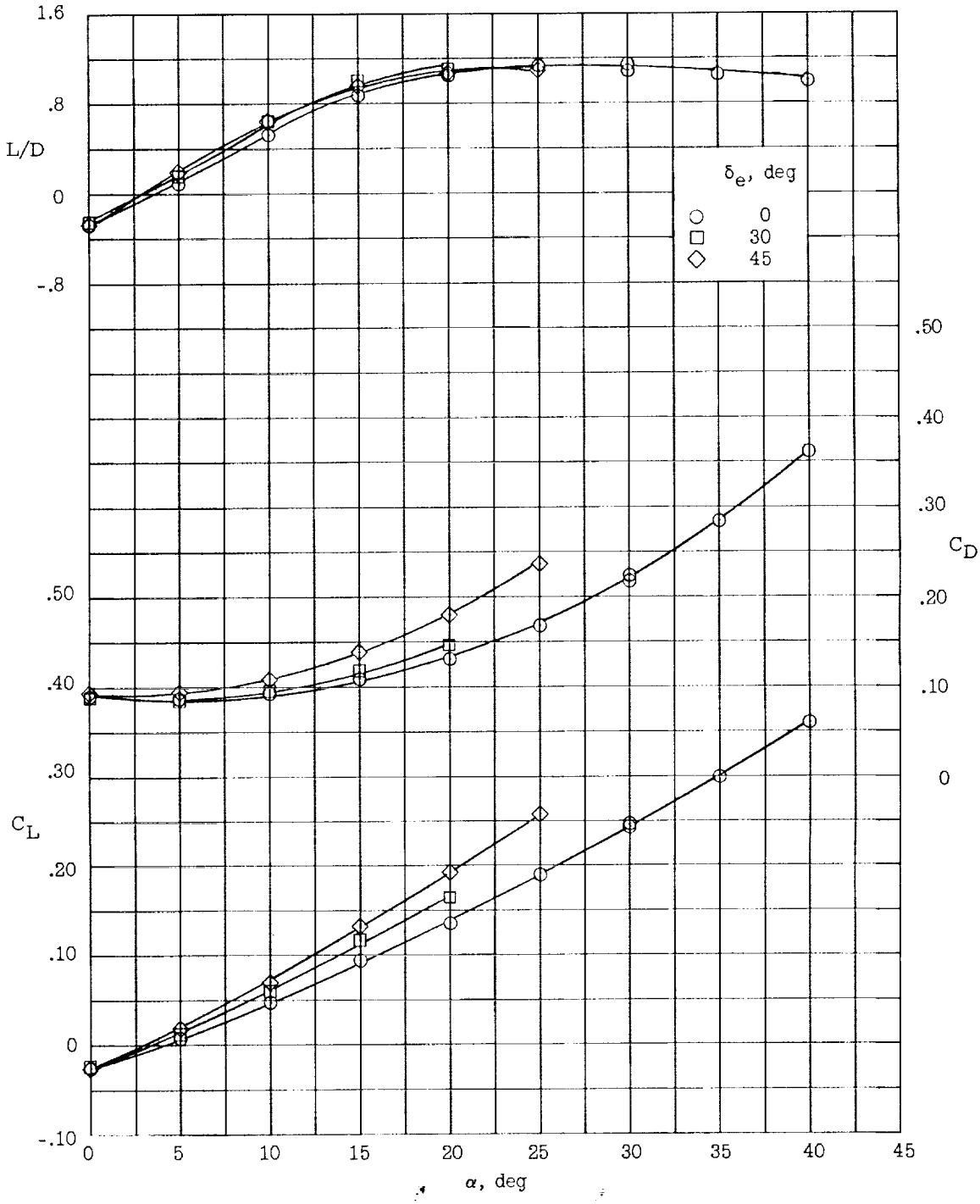

(a) Longitudinal performance characteristics.

Figure 5.- Longitudinal aerodynamic characteristics of configuration HL-10 with tip dorsal fins (fin A).

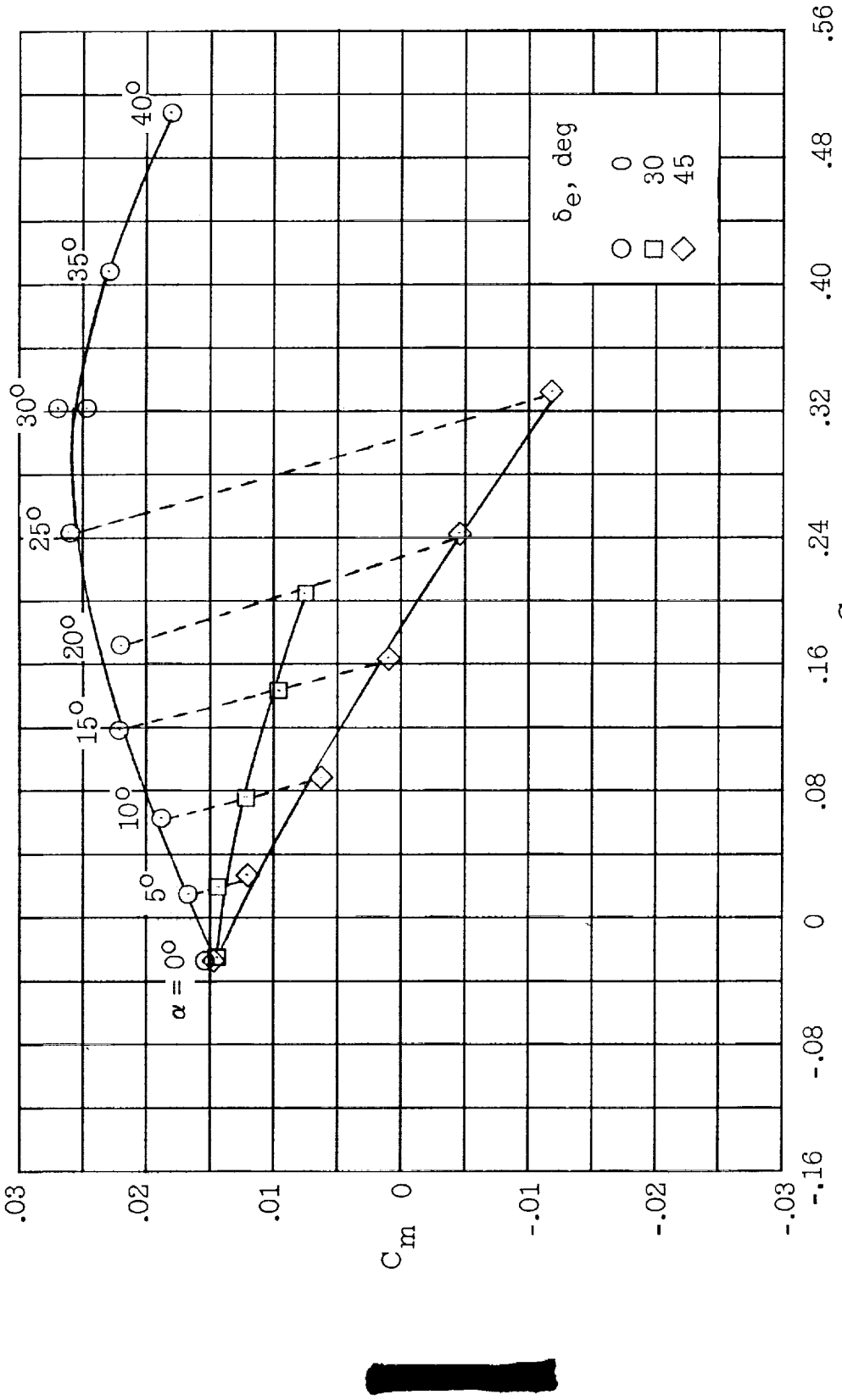

(b) Stability characteristics.

Figure 5.- Concluded.

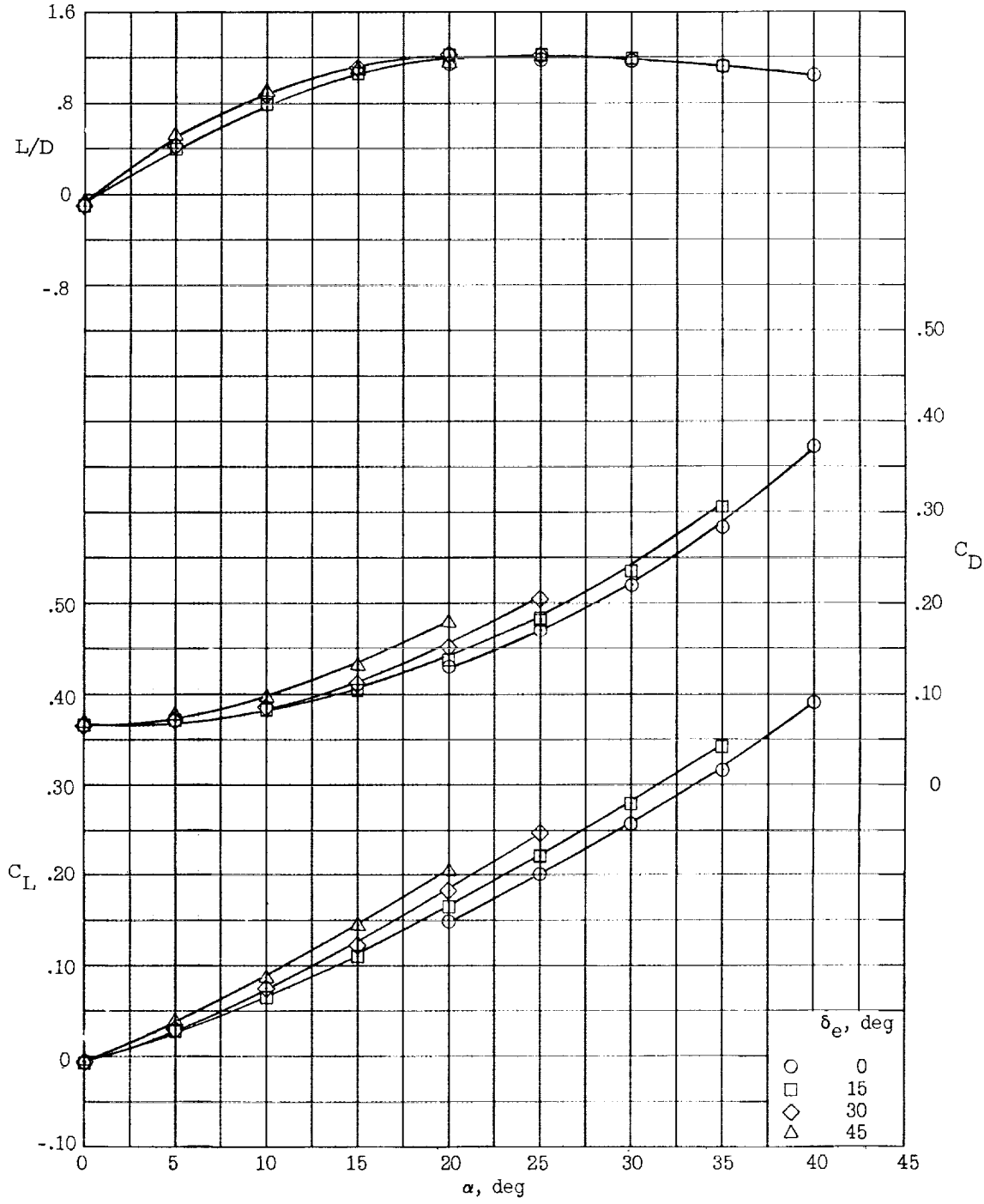

(a) Longitudinal performance characteristics.

Figure 6.- Longitudinal aerodynamic characteristics of configuration HL-10 with tip ventral fins (fin B) for various elevon deflection angles.

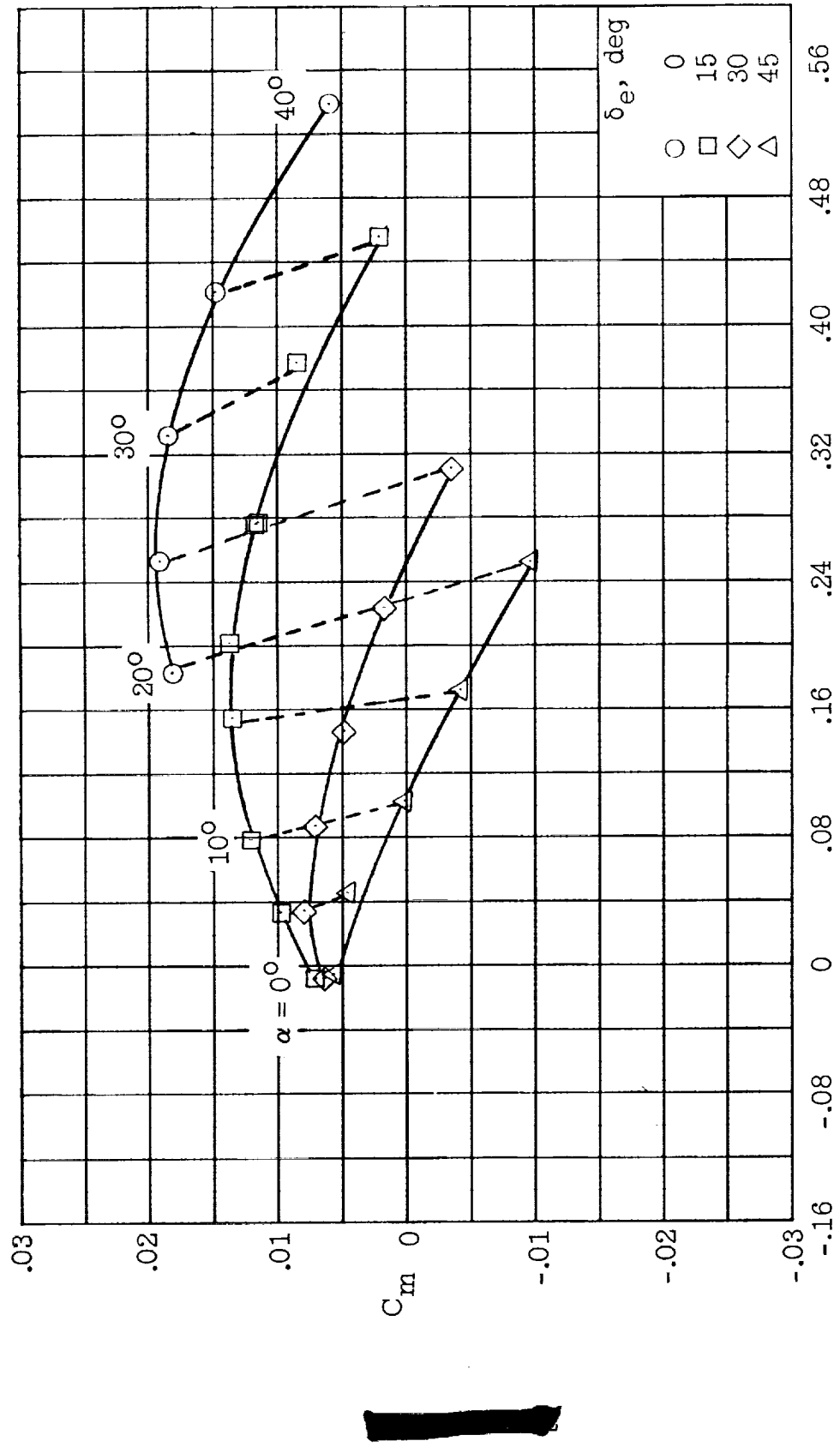

(b) Stability characteristics.

Figure 6.- Concluded.

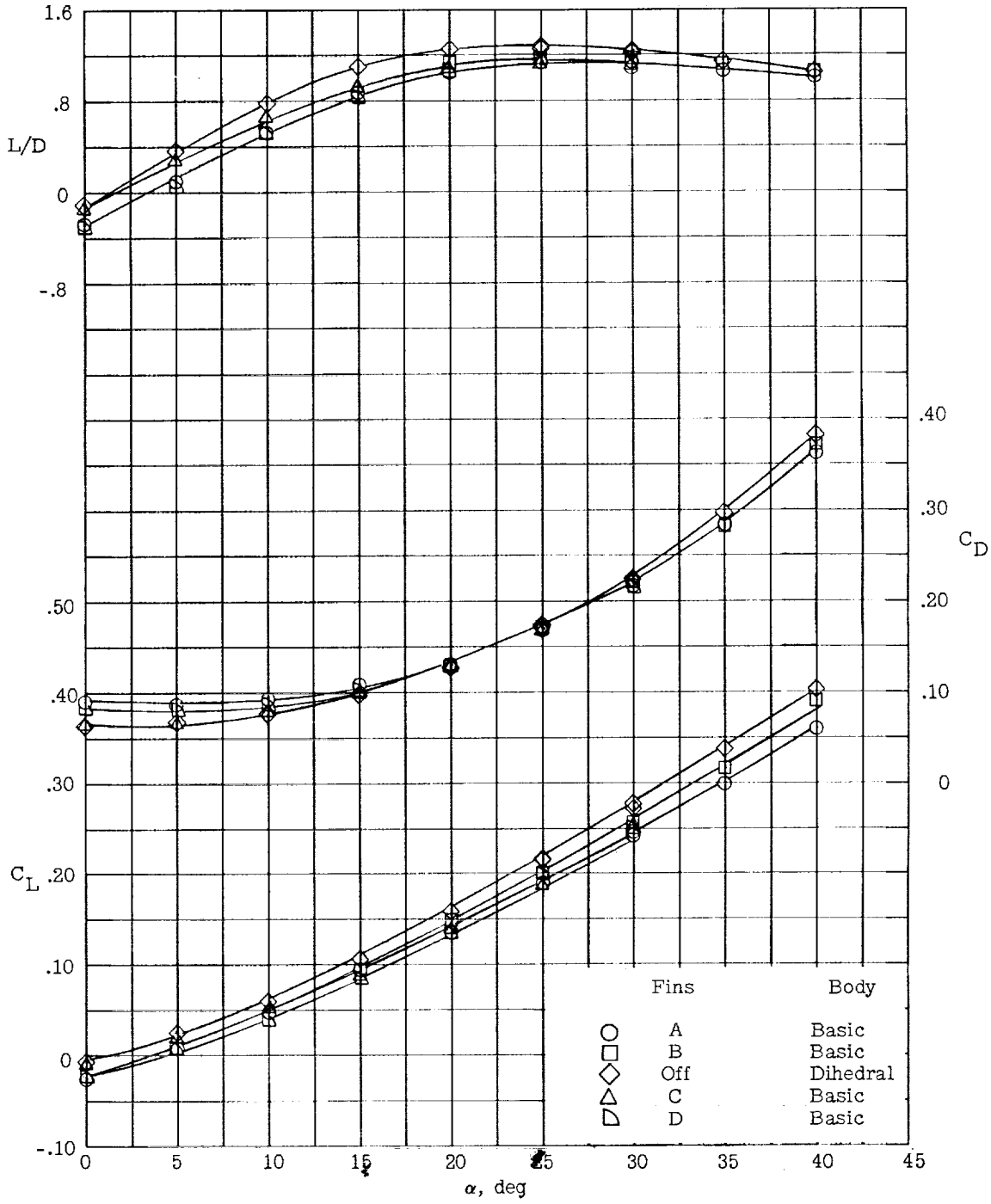

(a) Longitudinal performance characteristics.

Figure 7.- Comparison of longitudinal aerodynamic characteristics of various configurations. $\delta_e = 0^o$.

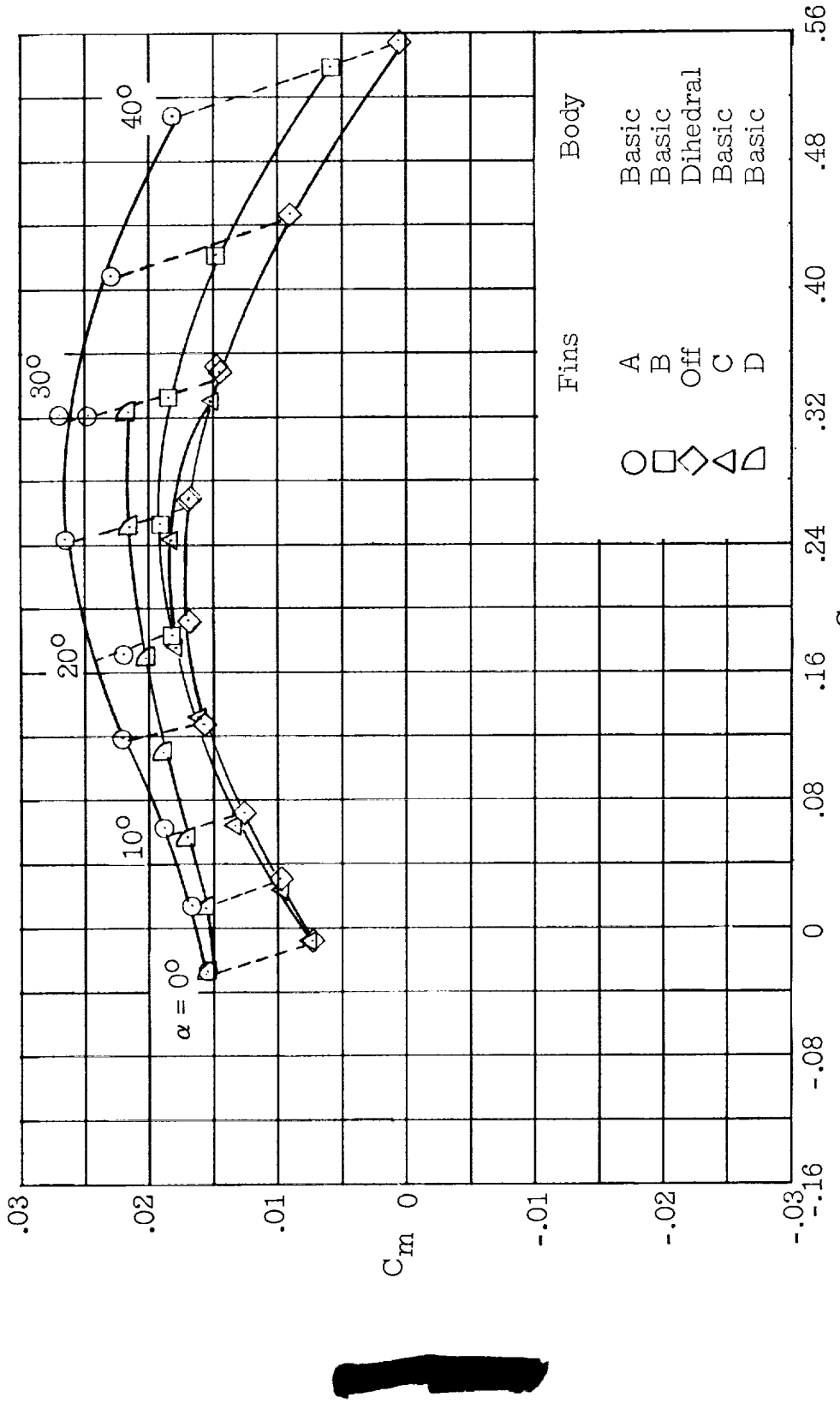

(b) Stability characteristics.

Figure 7.- Concluded.

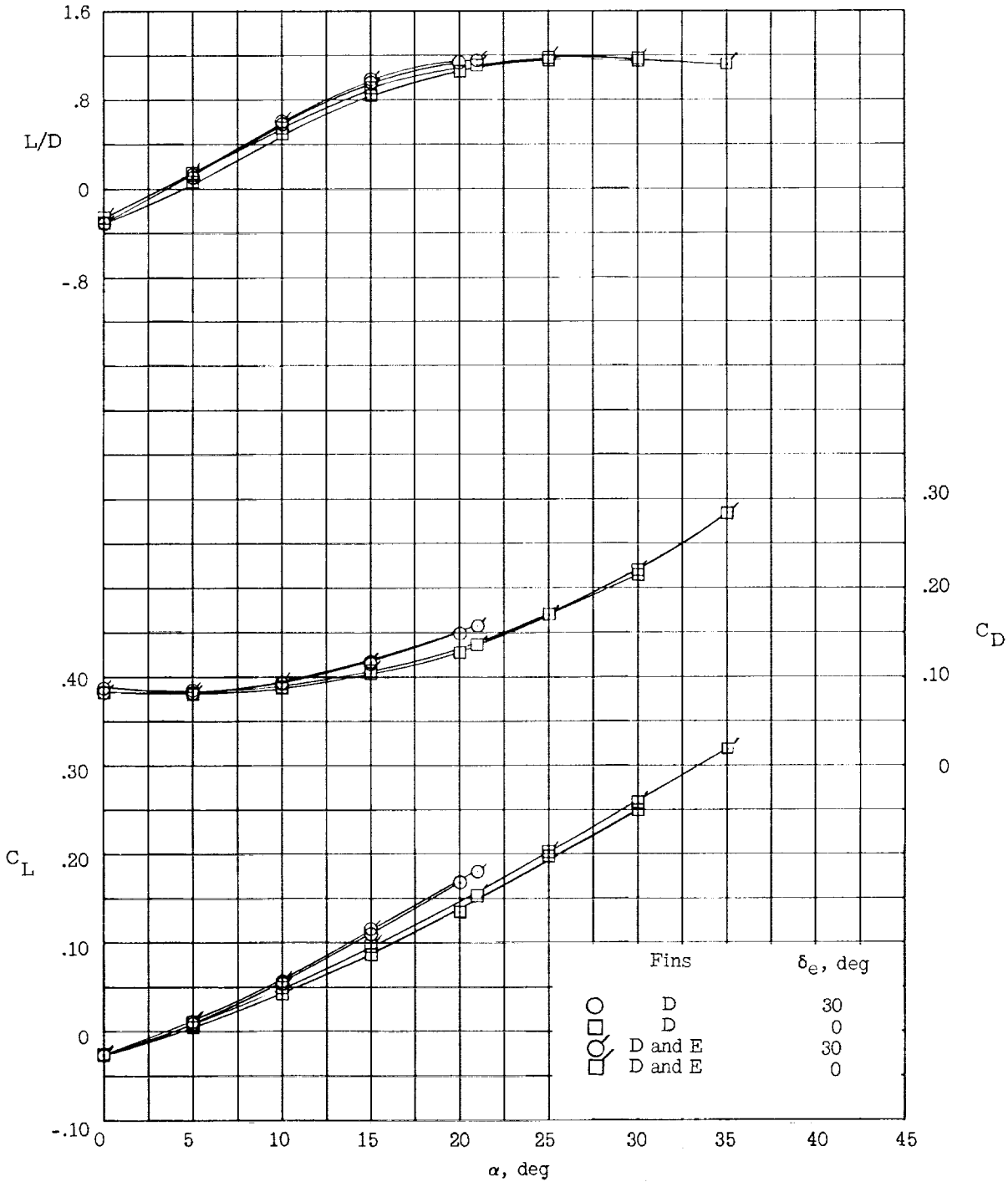

(a) Longitudinal performance characteristics.

Figure 8.- Effects on aerodynamic characteristics of adding center-line dorsal fin (fin E) to configuration with rolled-out tip dorsal fins (fin D).

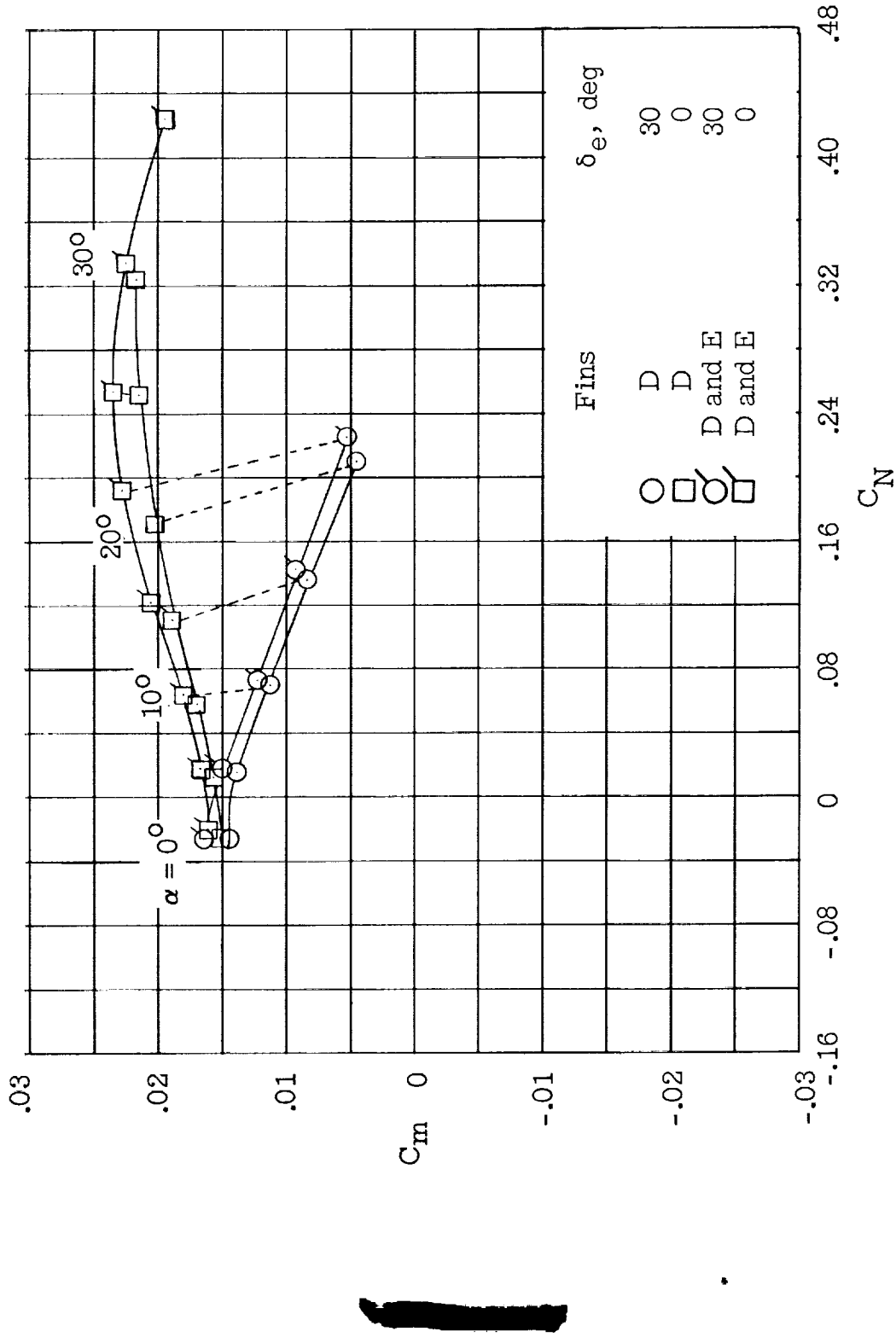

(b) Stability characteristics.

Figure 8.- Concluded.

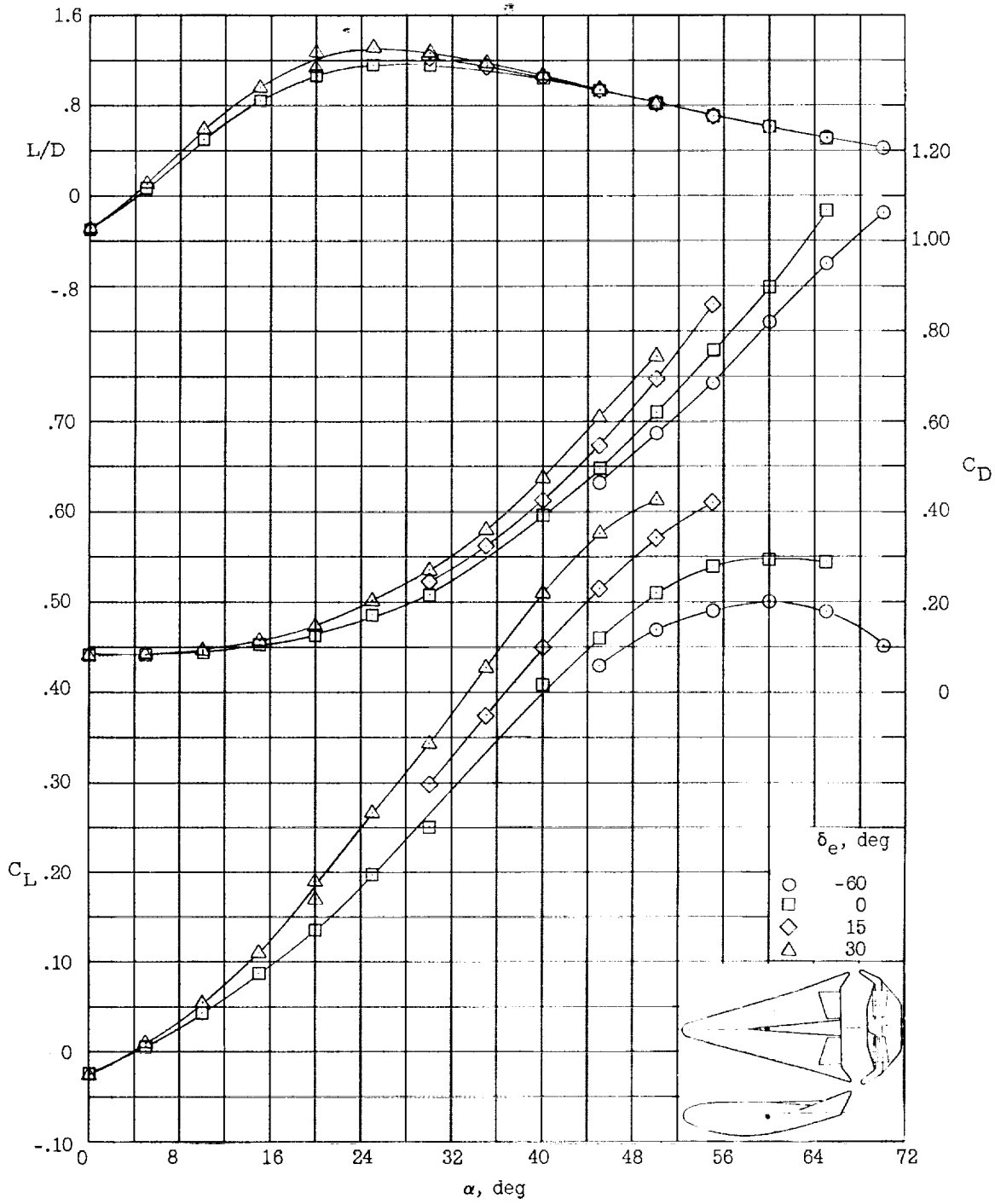

(a) Longitudinal performance characteristics.

Figure 9.- Longitudinal aerodynamic characteristics of configuration HL-10 with rolled-out tip dorsal fins (fin D) for various elevon deflection angles.

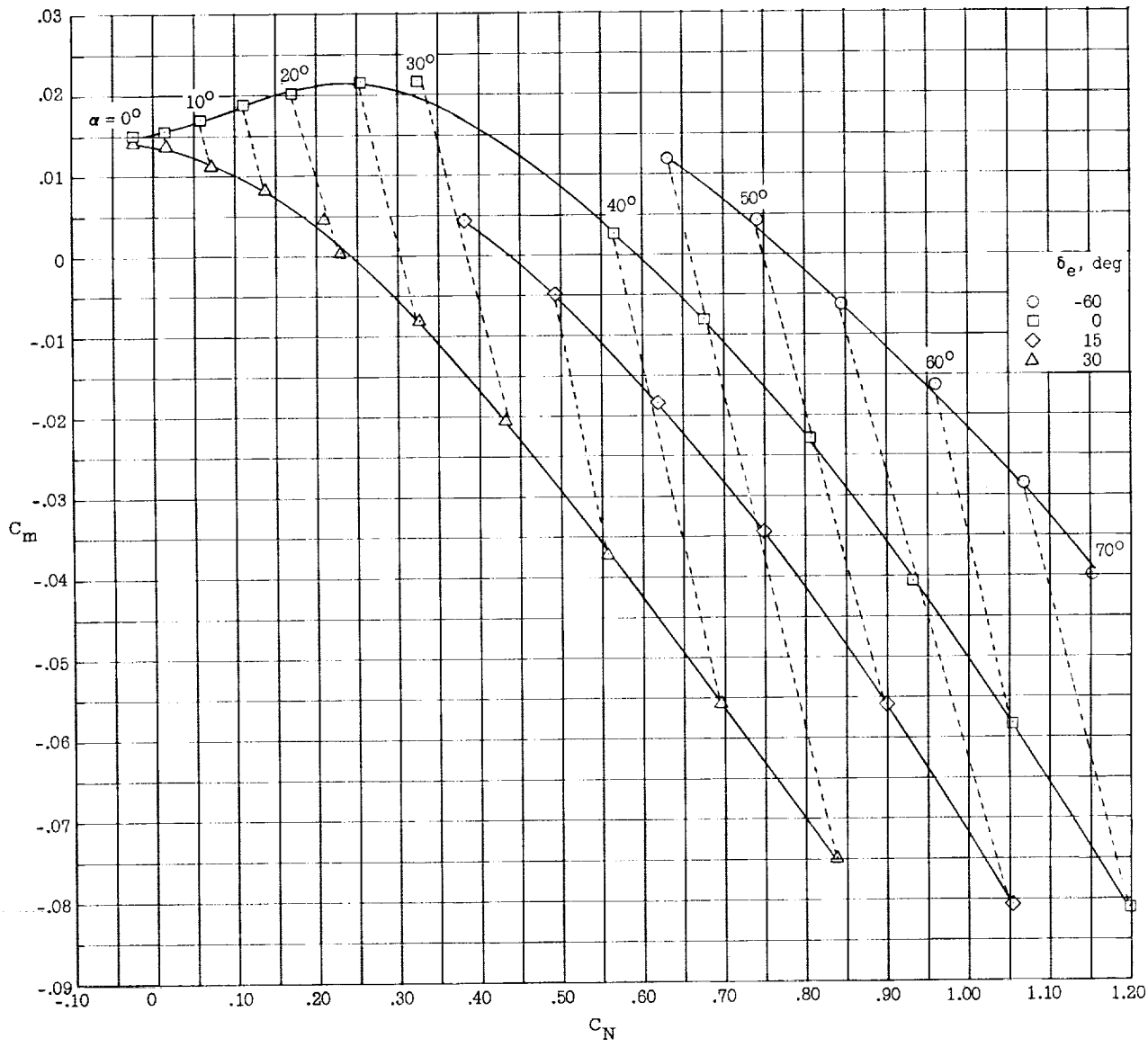

(b) Stability characteristics.

Figure 9.- Concluded.

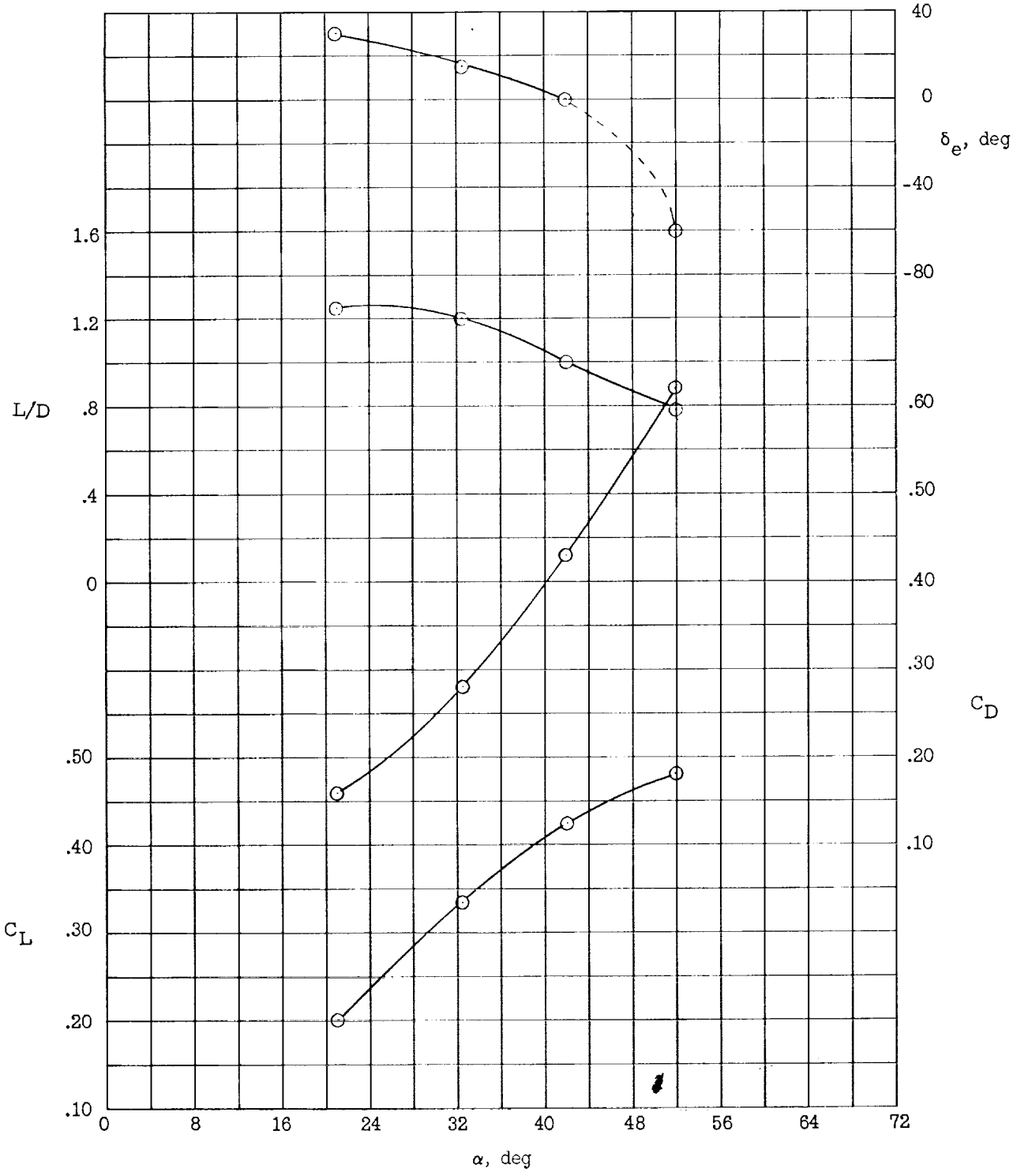

Figure 10.- Trimmed longitudinal aerodynamic characteristics of configuration with rolled-out tip dorsal fins (fin D).

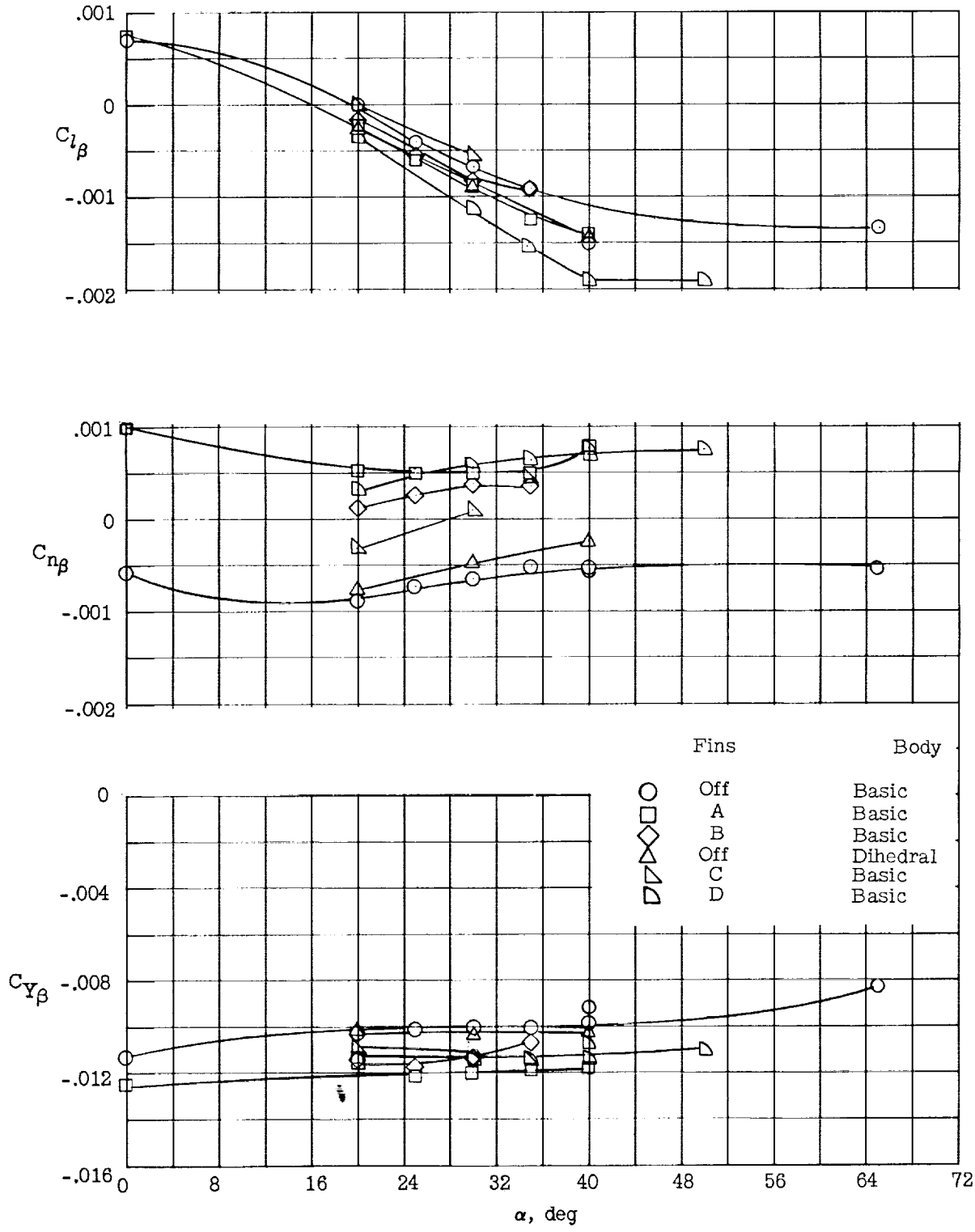

Figure 11.- Lateral and directional stability characteristics of various configurations. $\delta_e = 0^\circ$.

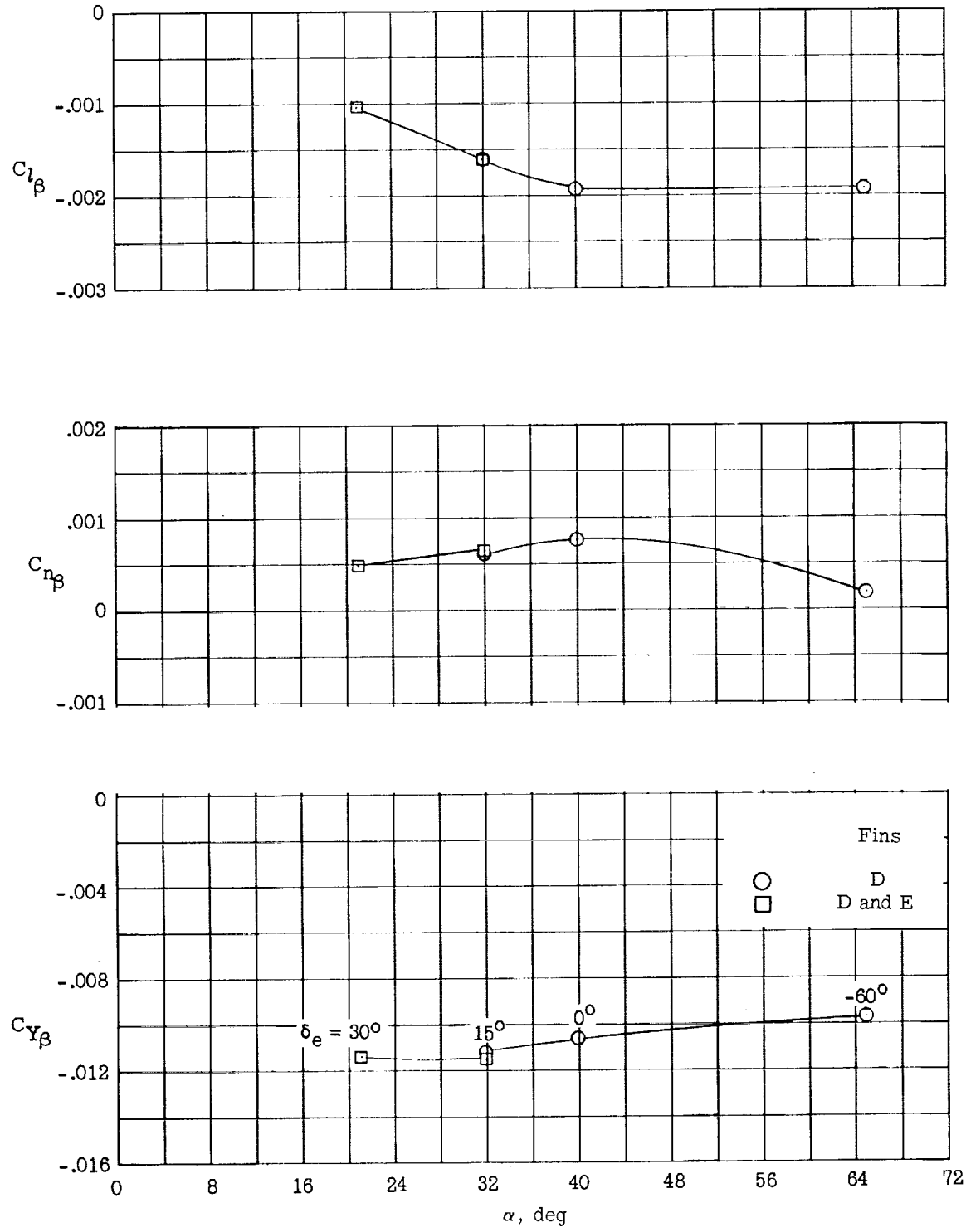

Figure 12.- Lateral and directional stability characteristics of two configurations with elevons deflected to approximate trim conditions.

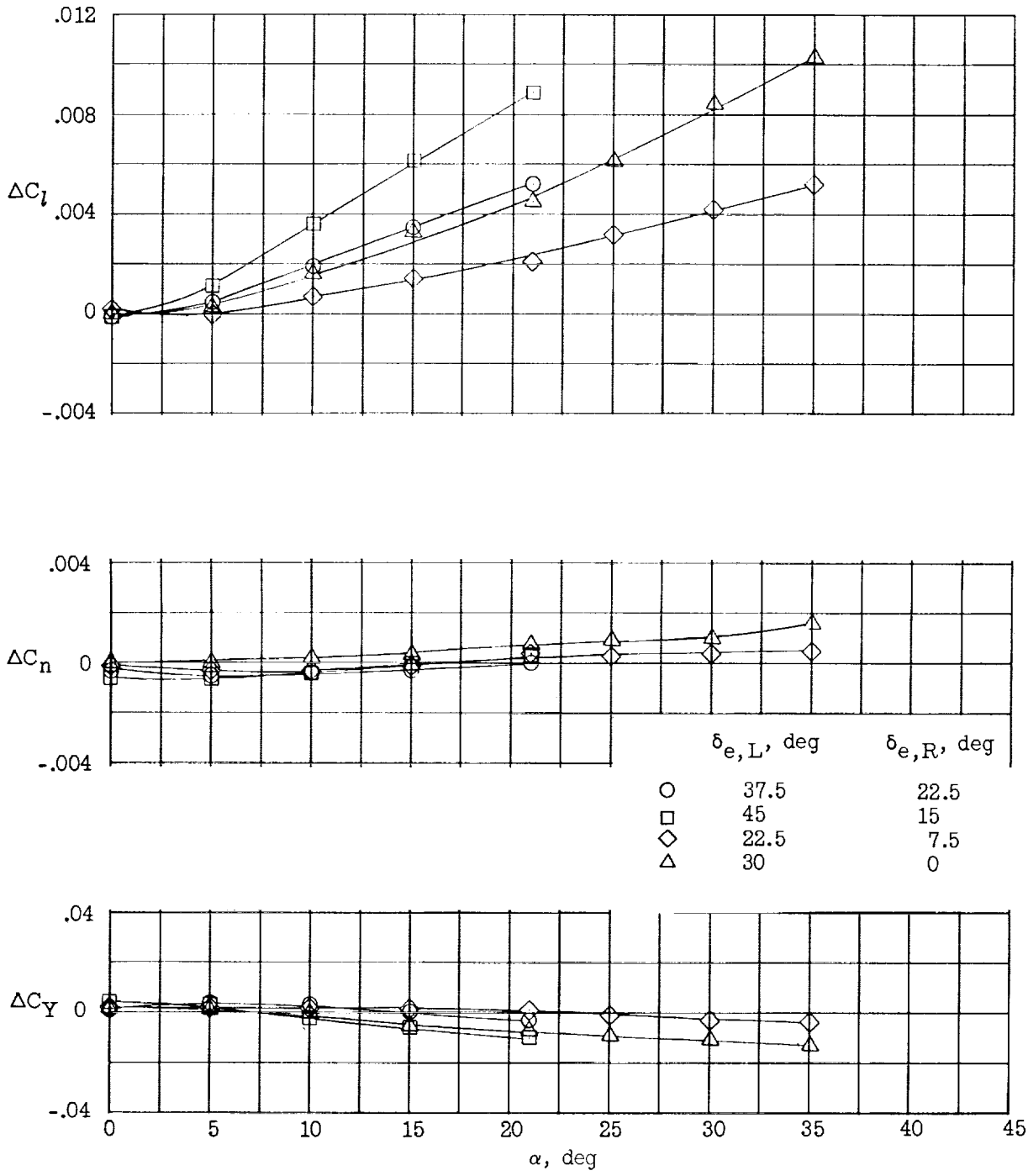

(a) Control inputs.

Figure 13.- Lateral control characteristics of configuration with rolled-out tip dorsal fins (fin D) and center-line dorsal fin (fin E).

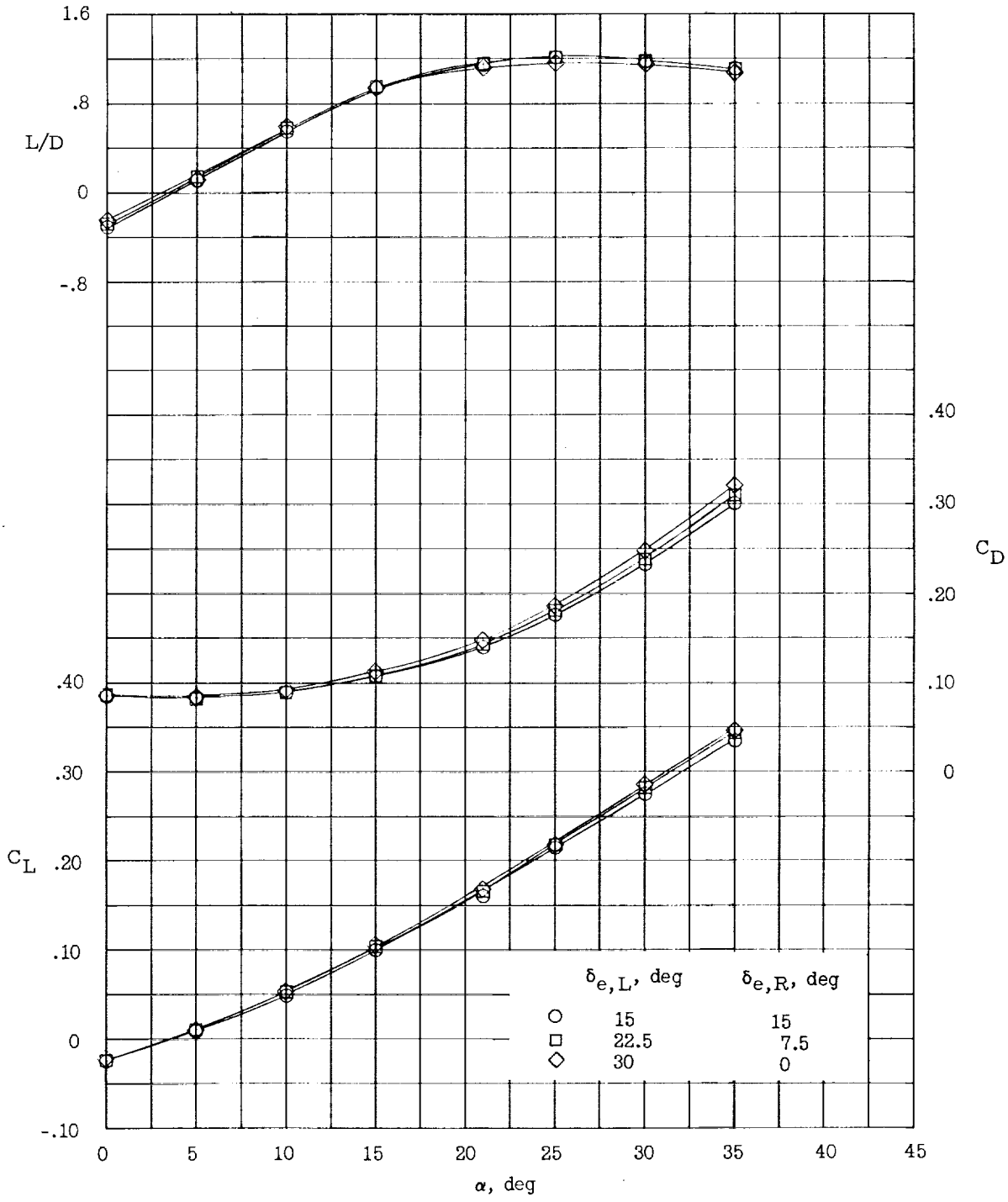

(b) Effects on longitudinal performance.

Figure 13.- Continued.

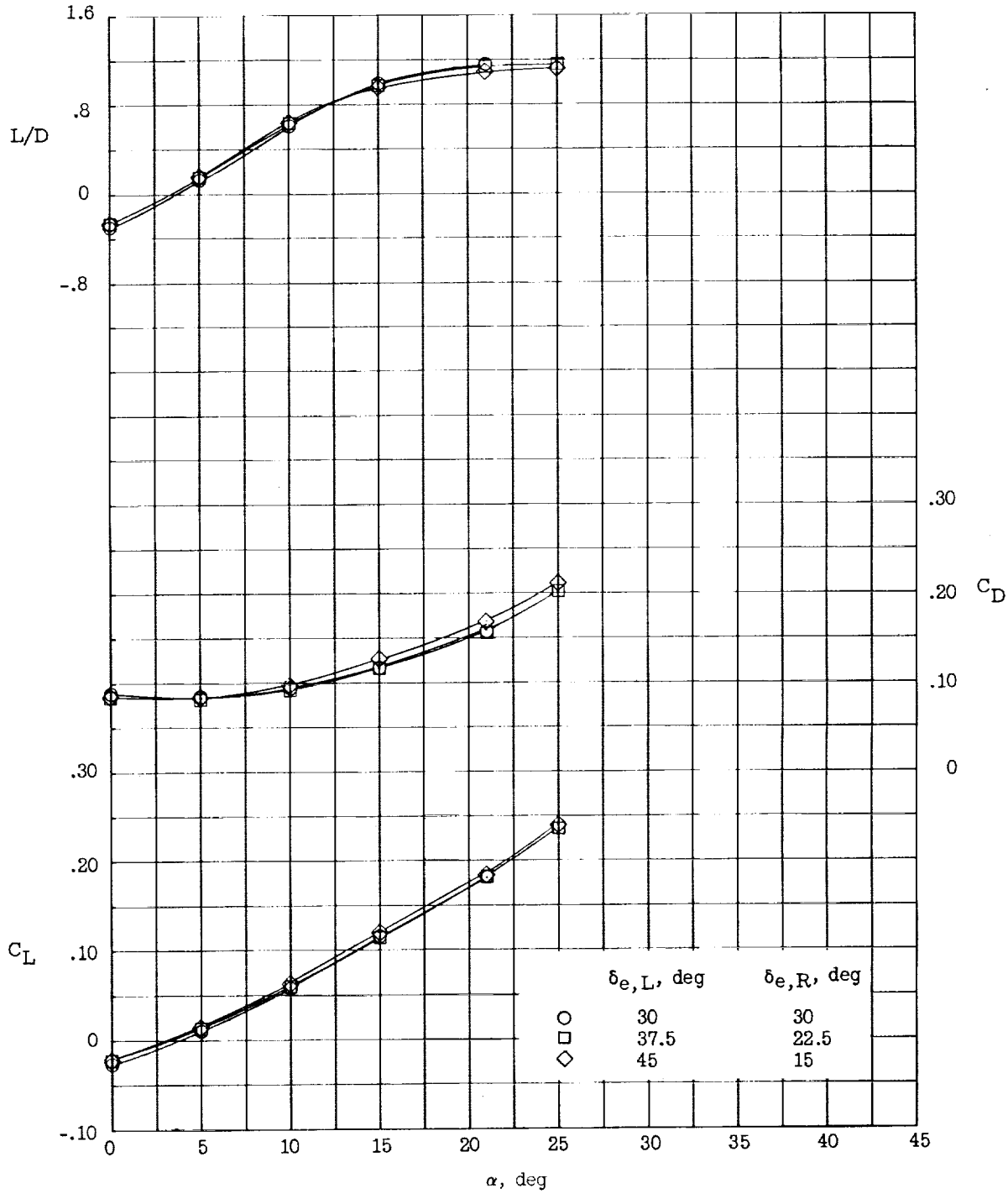

(b) Concluded.

Figure 13.- Continued.

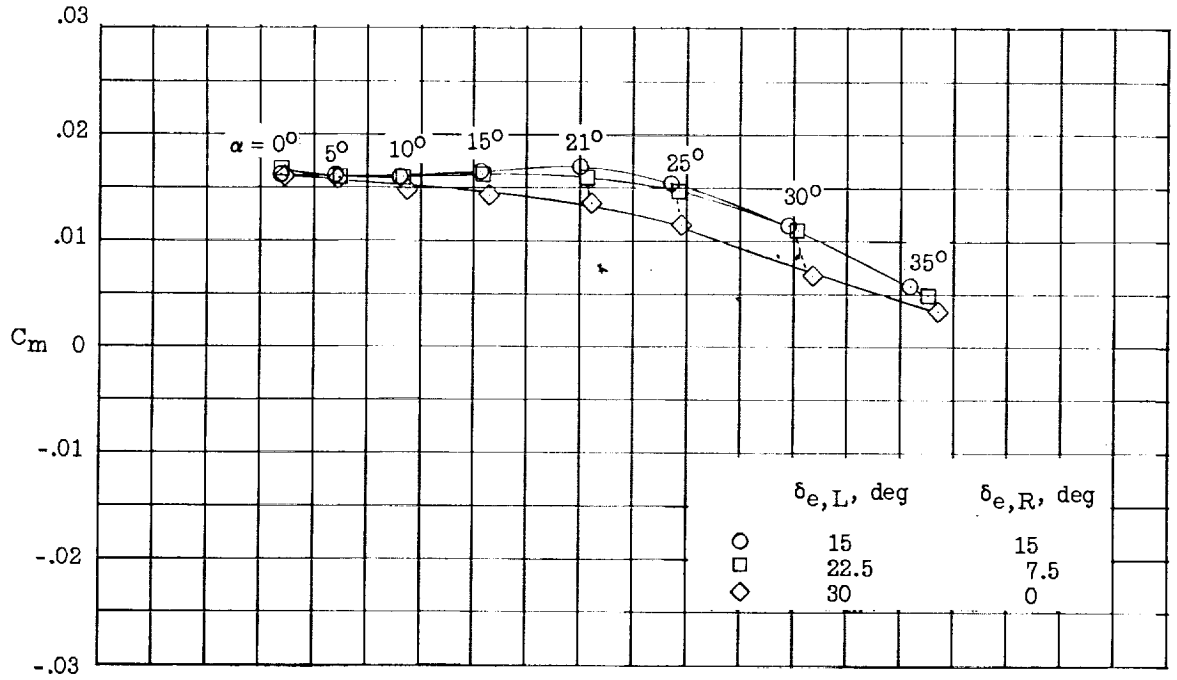

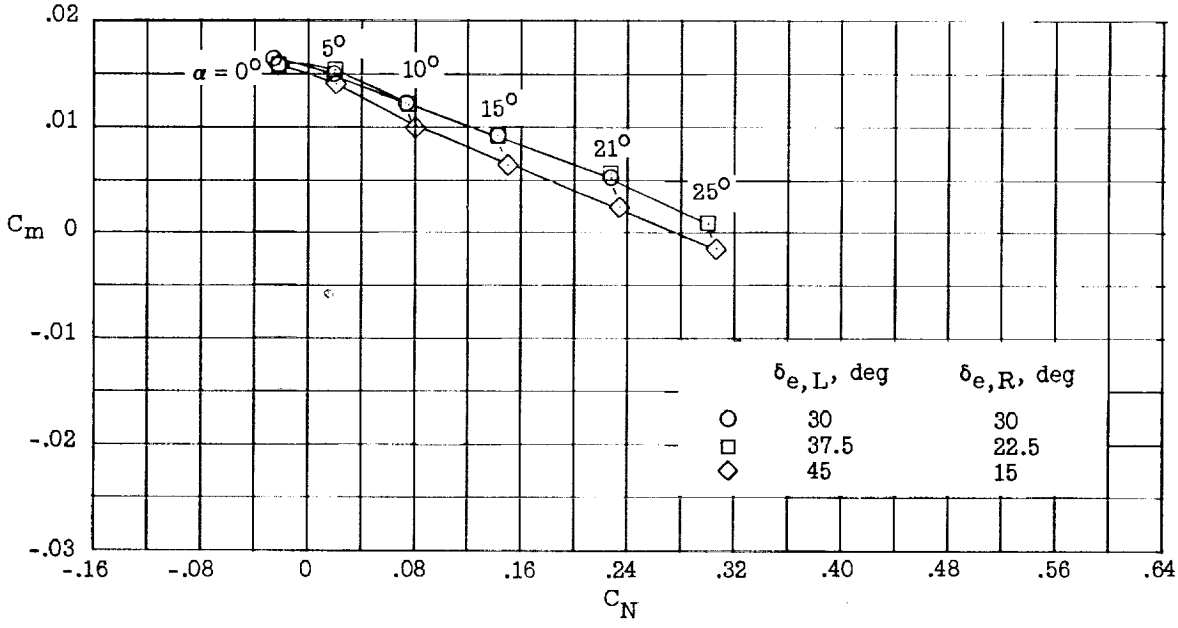

(c) Effects on stability.

Figure 13.- Concluded.

[redacted]

[redacted]